The Information Content of Pore Fluid $\delta^{18}O$ and $[Cl^-]$

MADELINE D. MILLER,* MARK SIMONS, JESS F. ADKINS, AND SARAH E. MINSON

California Institute of Technology, Pasadena, California

(Manuscript received 25 September 2014, in final form 15 May 2015)

ABSTRACT

Paleoceanographic proxies indicate that the ocean state during the Last Glacial Maximum (LGM) differed from the modern ocean state. Depth profiles of ocean sediment pore fluid $\delta^{18}O$ and $[Cl^-]$ have been used to reconstruct the $\delta^{18}O$ and salinity at the LGM. Here, it is investigated whether pore fluid profiles can constrain ocean $\delta^{18}O$ and salinity at other times and, simultaneously, their ability to constrain the LGM $\delta^{18}O$ and salinity. An inverse framework is developed that relies on Bayesian parameter estimation, thus allowing formal separation of prior assumptions from the information in observations. Synthetic problems are used to explore the information about past ocean tracers that can be recovered from pore fluid profiles. It is concluded that prior knowledge of deep ocean mixing time scales is essential to an accurate inverse estimate of LGM ocean salinity and $\delta^{18}O$ from modern pore fluid profiles. The most recent 10 000 years of ocean salinity and $\delta^{18}O$ and the error in their estimates are better constrained by the pore fluid profiles than are the LGM values. The inverse estimate of salinity and $\delta^{18}O$ is strongly correlated with the estimate of diffusivity of oxygen isotopes and $[Cl^-]$ in sediment pore fluids. Uncertainty on the diffusivity of oxygen isotopes and chloride in sediments is reduced through inversion of the pore fluid profiles, but simultaneous estimation of $\delta^{18}O$ or salinity and diffusivity increases the total uncertainty. The error reported in previous work may underestimate the true uncertainty of LGM deep ocean salinity and $\delta^{18}O$.

1. Introduction

Combining constraints from sediment pore fluid profiles of $\delta^{18}O$ and $[Cl^-]$ with $\delta^{18}O$ of carbonate of benthic foraminifera shells ($\delta^{18}O_c$), Adkins et al. (2002) inferred that there were larger-than-modern density differences between deep ocean water masses at the Last Glacial Maximum (LGM), a period lasting from 23 to 19 thousand years before present (ka BP; MARGO Project Members 2009), and that differences in density were due primarily to salinity. Of the ocean water masses considered, Adkins et al. (2002) concluded that Glacial Southern Source Bottom Water (GSSBW), deep water originating from the Southern Hemisphere, was the densest due to its high salinity. These results contrast strikingly with the distribution of today's deep ocean water masses whose density differences are set primarily by temperature; modern southern source bottom water, Antarctic Bottom Water (AABW), is the densest deep ocean water mass because it is cold, while remaining less saline than overlying water masses [see discussion in Miller et al. (2012)].

Larger density differences between northern source deep water and southern source bottom water imply higher vertical stratification. A greater vertical stratification would help explain indications that there was a physically isolated reservoir of CO_2 in the deep ocean at the LGM (Broecker and Barker 2007). While the LGM distribution of $\delta^{13}C$, Cd/Ca, and $\delta^{18}O$ possibly indicates a different-than-modern ocean circulation (e.g., Marchal and Curry 2008; Lund et al. 2011), the LGM ocean distributions of these properties may also be consistent with a modern circulation and differences in surface forcing (e.g., Gebbie 2012; Gebbie and Huybers 2006; LeGrand and Wunsch 1995). Improved constraints on ocean temperature and salinity in the past would facilitate the disentanglement of physical changes from chemical and biological signals and better explain why tracer fields in the past ocean varied so strikingly from those of today's ocean.

* Current affiliation: Department of Earth and Planetary Sciences, Harvard University, Cambridge, Massachusetts.

Corresponding author address: Madeline D. Miller, Department of Earth and Planetary Sciences, Harvard University, 20 Oxford St., Cambridge, MA 02138.
E-mail: madelinemiller@fas.harvard.edu

DOI: 10.1175/JPO-D-14-0203.1

The search for reliable proxies of past deep ocean temperature and salinity has proved difficult. In theory, pore fluid reconstructions of past $\delta^{18}O$ and $[Cl^-]$ have a unique advantage over other paleoceanographic proxies of temperature and salinity in that they respond only to physical changes in the ocean. However, so far pore fluid profiles of $\delta^{18}O$ and $[Cl^-]$ have only been used to reconstruct the temperature and salinity at a single point in time: the LGM. To fully understand the changing ocean circulation over the most recent deglaciation, we must know the temporal evolution of temperature and salinity fields. Here we investigate whether pore fluid profiles can constrain the ocean $\delta^{18}O$ and $[Cl^-]$ at other points in time. Simultaneously, we investigate the extent to which they actually constrain the LGM $\delta^{18}O$ and $[Cl^-]$.

In their reconstructions of LGM $\delta^{18}O$ and $[Cl^-]$, Lado Insua et al. (2014), Malone et al. (2004), Adkins et al. (2002), Schrag et al. (2002), Adkins and Schrag (2001), Paul et al. (2001), Schrag et al. (1996), Schrag and DePaolo (1993), and McDuff (1985) relied on a number of restrictive assumptions that made it impossible to recover histories of $\delta^{18}O$ and $[Cl^-]$ at any time other than the LGM. They supposed that $\delta^{18}O$ and $[Cl^-]$ are both conservative tracers in ocean sediments subject to one-dimensional advection and diffusion.[1] All of the parameters of the problem were assumed known except the bottom water histories of both $\delta^{18}O$ and $[Cl^-]$. These histories determine the concentration boundary condition time series at the sediment–water interface. They further assumed that the basic shape of the bottom water histories was known up to a scaling constant; that is, the bottom water histories of $\delta^{18}O$ and $[Cl^-]$ primarily tracked changes in $\delta^{18}O$ of benthic foraminiferal calcite, benthic $\delta^{18}O_c$, and sea level, but were able to scale relative to an LGM-to-modern difference in concentration. This scaling parameter was then varied in order to find a good fit between the modeled output and the measurements (Fig. 1). Three different salinity histories resulting from three choices for the LGM-to-modern scaling parameter are shown in Fig. 1a. The modern pore fluid profile data that would result from the application of each of these histories as the bottom water boundary condition are plotted on top of measurements [Ocean Drilling Program (ODP) site 1093] in Fig. 1b. The reported value of the LGM salinity was determined from the LGM-to-modern scaling parameter that yielded pore fluid profiles with the best fit to the measurements. Thus, the deglacial history at each site was fixed to a composite benthic $\delta^{18}O_c$ record and sea level curve, scaled by a spatially variable (site specific) constant.

Today the bulk of the ocean interior is weakly stratified, such that the deep ocean salinity and $\delta^{18}O$ are everywhere very close to their mean ocean values. However, coupling the local time series to the global mean time series implicitly assumes that changes in total ocean water volume always produce the same local change in properties. Further, this approach requires that all sites coevolve in the same way at all times. Tying bottom water histories at all sites proportionally to the mean sea level curve prohibits them from expressing independent temporal evolution as they approach present day values. Finally, this assumption requires that there is a linear relationship between a site's concentration and the global mean. Adkins et al. (2002) note that their best fit models generate systematic misfits between all of the data and model-generated profiles in the upper sediment column, implying that the pore fluid profiles contain information about the deglacial evolutions of temperature and salinity that could not be extracted with their methodology.

Previous pore fluid reconstructions of LGM $\delta^{18}O$ and $[Cl^-]$ have all assumed that the dominant diffusion coefficient D'_0 at a site can be determined independently of the bottom water boundary condition. The coefficient D'_0 was calculated as L^2/T, where $T = 20\,000$ years and L was the depth of the maximum value of $\delta^{18}O$ and $[Cl^-]$ in the sediments. For a maximum measured salinity at 40 m below sea floor (mbsf), this relation yields $D'_0 = 2.5 \times 10^{-5}\,cm^2\,s^{-1}$. Recent studies have shown that the LGM occurred at different times for different mountain glaciers and ice sheets, reaching their maxima between 33 and 26.5 ka BP and remaining stable until 19–14 ka BP (Clark et al. 2009), which calls into question both the idea of a synchronous LGM in the ocean and the timing of the LGM at any site in the ocean, particularly given that the ocean equilibration time scales may be up to 10 000 years or even longer (Wunsch and Heimbach 2008).

We develop an inverse framework to reconstruct past ocean bottom temperature and salinity from ocean sediment core interstitial water profiles of $\delta^{18}O$ and $[Cl^-]$ (in combination with $\delta^{18}O$ of carbonate of benthic foraminifera) that allows us to relax many of the assumptions listed above. In particular, we relax the assumption that bottom water histories scale to the sea level curve, allowing us to test the robustness of previous reconstructions and to examine the extent to which we can extract more information

[1] While there is significant two- or three-dimensional advective fluid flow in many places on the ocean floor associated with spreading and converging plate boundaries, submarine groundwater discharge from continental aquifers, gas seeps (Judd and Hovland 2007), and bathymetric pressure perturbations due to current–obstruction interactions (Huettel and Webster 2001), the evolution of pore fluid concentration profiles in impermeable muddy sediments in abyssal plains is dominated by one-dimensional diffusion (Spinelli et al. 2004; Huettel and Webster 2001; Boudreau 1997; Berner 1980).

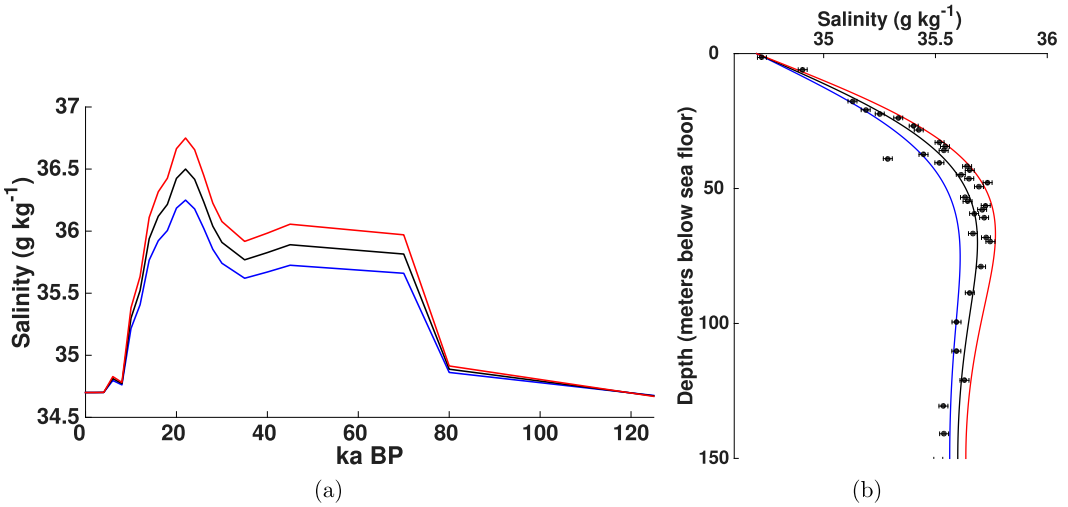

FIG. 1. Illustration of the method used in Adkins et al. (2002) to reconstruct the LGM salinity and δ^{18}O. Changes in bottom water salinity were assumed to scale to changes in the mean sea level. The scaling factor was adjusted until the pore fluid data produced by the hypothetical bottom water salinity time series closely matched the measured pore fluid data. Low sea level corresponds to high salinity and vice versa. (a) Bottom water salinity histories using three different scaling factors. (b) Forward model output in response to the bottom water histories, overlaid on measured [Cl^-] data {black circles, converted from [Cl^-] to S using the relation $S = (19.354/35)[Cl^-]$} in sediment pore fluids at ODP site 1093 (49°58.6′S, 5°51.9′E; Shona Ridge). Each color corresponds to a different LGM–modern scaling factor.

than the LGM salinity and δ^{18}O from present-day interstitial water profiles. This new approach to the problem allows us to simultaneously reevaluate the information about the LGM yielded by the pore fluid profiles.

There are infinite bottom water histories that could have generated our observations; the inverse problem is nonunique. However, some of the mathematically acceptable histories may be physically implausible. For example, negative salinities in the inverse solution time series are mathematically possible but physically impossible. Therefore, we seek the full distribution of physically acceptable bottom water time series that could have generated our measurements. Our approach relies on a Bayesian Markov chain Monte Carlo (MCMC) method to reconstruct a distribution of bottom water histories that could generate modern pore fluid profiles of δ^{18}O and [Cl^-]. A Bayesian approach allows us to easily restrict our solution space. The Bayesian approach also explicitly allows us to separate our prior assumptions and uncertainty from information contained in the measurements and to recover a distribution of inverse solutions with varying probabilities. MCMC techniques allow us to consider the fully non-Gaussian and nonlinear problem, in which we invert for physical parameters such as the diffusion coefficient with arbitrary prior distributions, in a manner robust to local minima and maxima of the inverse solution space. The particular algorithm we use is named the Cascading Adaptive Transitional Metropolis in Parallel (CATMIP; Minson et al. 2013), which is one example of the general class of Bayesian MCMC algorithms.

We first describe our methodological approach to the forward and inverse problems and explain how we encapsulate our knowledge about the deep ocean as probability distributions that can be supplied to a Bayesian MCMC sampler. With synthetic examples, we then evaluate what information about past bottom water histories can be recovered from modern pore fluid profiles of δ^{18}O and [Cl^-]. In a separate manuscript, we use what we have learned from synthetic examples to invert real data and demonstrate the robust and nonrobust oceanographic constraints that can be recovered from existing pore fluid profiles.

For convenience in the text we often refer to [Cl^-] as salinity or S, using the conversion factor $S = (19.354/35)[Cl^-]$; however, all of the data measurements are derived from pore fluid [Cl^-]. In our synthetic examples, we consider the evolution of salinity, but our conclusions apply equally to reconstructions of both δ^{18}O and S, as well as other conservative tracers.

2. Problem framework and inverse approach

a. *Forward problem*

In the following section, we outline the derivation of the advection–diffusion equation for the time evolution of pore fluid concentration. For more complete treatment

of the assumptions and equations, we refer the reader to Berner (1980) and Boudreau (1997). We assume that $[Cl^-]$ and $\delta^{18}O$ are chemically inert and that there are no significant local horizontal gradients in the sediment properties. The vertical distribution of each individual tracer c then evolves in time according to a one-dimensional advection–diffusion equation:

$$\frac{\partial(\phi c)}{\partial t} = \frac{\partial}{\partial z}\left(D_0 \frac{\phi}{\theta^2}\frac{\partial c}{\partial z}\right) - \frac{\partial(u\phi c)}{\partial z}, \quad (1)$$

where ϕ is the sediment porosity (water volume/bulk volume), θ is the sediment tortuosity (traveled distance of diffused ion/direct distance between spaces), and D_0 is the diffusivity in water of the chemical species of interest. The variable D_0 is a function of temperature and ionic strength, which both can be functions of depth and time in ocean sediments. The variability of D_0 with temperature is well-predicted by the Stokes–Einstein relation $(D_0\eta_0/T)|_{T_1} = (D_0\eta_0/T)|_{T_2}$, where η is the temperature-dependent viscosity of the water and T is the absolute temperature. Thus, $D_0 = rD_{0,T=20°C} = rD_0'$, where r is a function of temperature. Here we take D_0' to be an unknown constant and use the temperature measurements logged downhole at the time of drilling to compute r, assuming that the vertical gradient of temperature is steady. The variable u is the vertical velocity of the pore water with respect to the sediment–water interface, which is predominantly due to sediment compaction, and z is the depth in the sediment, defined as increasing downward.

If we assume steady-state compaction ($\partial\phi/\partial t = 0$) and incompressible flow [$\partial(\phi u)/\partial z = 0$], Eq. (1) simplifies to

$$\phi\frac{\partial c}{\partial t} = \left(\frac{\partial D^*}{\partial z} - \phi u\right)\frac{\partial c}{\partial z} + D^*\frac{\partial^2 c}{\partial z^2}, \quad (2)$$

where $D^* = D_0(\phi/\theta^2)$. A typical model for θ^2 is $\theta^2 = \phi f$, where f is the nondimensional formation factor:

$$f = \frac{\text{bulk sediment specific electrical resistivity}}{\text{porewater resistivity}}. \quad (3)$$

Laboratory measurements suggest that a good approximation for f is ϕ^{-n}, where an average value of n over various sediments is 1.8 (Berner 1980). Our final equation describing concentration evolution with time and space is

$$\frac{\partial c}{\partial t} = \left[D_0'\left(\phi^{0.8}\frac{\partial r}{\partial z} + 1.8\phi^{-0.2}r\frac{\partial \phi}{\partial z}\right) - u\right]\frac{\partial c}{\partial z} + r\phi^{0.8}D_0'\frac{\partial^2 c}{\partial z^2}, \quad (4)$$

where ϕ in our model is a smoothed version of the measured porosity in each core. Assuming that compaction ceases at some depth in the sediment [$(\partial\phi/\partial z)|_{z=-H} = 0$] and that compaction is at steady state ($\partial\phi/\partial t = 0$), u can be derived from the constant sedimentation rate and porosity data. At the depth of no compaction H, the fluid velocity u and the sediment burial velocity w are the same, that is, $u_H = w_H$ and $\partial u/\partial z = 0 = \partial w/\partial z$. Then, by continuity, $\phi u = \phi_H u_H = \phi_H w_H$, or $u = (\phi_H w_H)/\phi$. The variable w_H is the constant sedimentation rate, determined by dating the sediment core. The vertical concentration profile is modeled according to Eq. (4), with a concentration profile as the initial condition and with two boundary conditions. The top (ocean–sediment interface, at $z = 0$ m) boundary condition is the ocean bottom water history overlying the core site that we seek to constrain. At the lower boundary ($z = 350$ m), we assign a gradient boundary condition. The evolution of Eq. (4) is heavily dominated by diffusion, making it a stiff partial differential equation. We numerically solve the equation with a second-order implicit–explicit (IMEX) method, in which the advection terms are solved explicitly while the diffusion terms are solved implicitly (Ascher et al. 1995). The time step in the solver is 10 years and the spatial resolution is 50 cm. The total integration time is 125 000 years. Over the integration time of 125 000 years and 350 m of sediment, these choices lead to a two-norm combined round-off and truncation error in the solution of $O(10^{-4})$ g kg^{-1}. This error estimate is derived from integration of an analogous one-dimensional advection–diffusion equation with constant coefficients to which there is a known analytical solution.

b. *Inverse problem*

In practice, we measure the modern concentration depth profile $c(z)|_{t=\text{mod}}$, and from this set of observations we infer the past time evolution of water properties at the ocean sediment–water interface, $c_0(t)$. We can write this problem in general as

$$G(\mathbf{m}) = \mathbf{d}_{\text{obs}}, \quad (5)$$

where $\mathbf{m}$ represents the unknown boundary conditions; $\mathbf{d}_{\text{obs}}$ is the measured data [$c(z)|_{t=\text{mod}}$], the pore fluid profile; and G is the forward model of advection and diffusion in the sediments. When we solve for boundary conditions only, Eq. (5) is a linear equation that can be written in terms of discrete Green's functions as a matrix–vector multiplication:

$$\mathbf{Gm} = \mathbf{d}_{\text{obs}}, \quad (6)$$

where the bold, Arial font indicates that $\mathbf{G}$ is a matrix rather than a function. We cannot invert the matrix $\mathbf{G}$ directly for $\mathbf{m}$, as the solution for $\mathbf{m}$ in both the continuous and discretized framework is an ill-posed problem (Hansen 1998).

We find traditional regularized or damped inverse methods insufficient for solving our particular ill-posed inverse problem. It is difficult to bound the bias in the inverse solution because of the choice of regularization. Further, inversion for the diffusion coefficient D_0' requires a nonlinear technique. Finally, as we know a priori from the structure of the problem that there exist infinite possible solutions, we seek to recover a distribution of physically reasonable solutions that can serve as an error estimate (Miller 2014).

c. *Bayes' theorem*

Though the inverse solutions to a diffusion problem are infinite, we may wish to exclude certain classes of solutions based on our prior knowledge. Using a Bayesian approach, we can restrict the solution space by applying our prior knowledge of the problem. Bayes' theorem states that

$$P(\mathbf{m}\,|\,\mathbf{d}_{\text{obs}}) \propto P(\mathbf{d}_{\text{obs}}\,|\,\mathbf{m})P(\mathbf{m}), \tag{7}$$

where $\mathbf{m}$ is a vector of input parameters and $\mathbf{d}_{\text{obs}}$ denotes the observations. Vector $\mathbf{m}$ is the set of unknowns we wish to solve for, in our case the ocean bottom water history of salinity or δ^{18}O and the unknown diffusion parameter D_0', and $\mathbf{d}_{\text{obs}}$ is the sediment pore fluid depth profile of measured concentrations. The probability that a given set of input parameters is correct, given the measured data, is proportional to the product of the prior probability of those input parameters and the likelihood of the data produced by the model using those input parameters. The prior probability $P(\mathbf{m})$ encompasses our knowledge of the input parameters independent of the measurements $\mathbf{d}_{\text{obs}}$. The likelihood $P(\mathbf{d}_{\text{obs}}\,|\,\mathbf{m})$ is computed using the differences between the measured data and output of the forward model using a given set of input parameters $\mathbf{m}$. The posterior probability distribution, or posterior, is $P(\mathbf{m}\,|\,\mathbf{d}_{\text{obs}})$.

d. *Bayesian estimation for a linear inverse problem with Gaussian prior parameters*

Assuming a linear model with Gaussian prior probabilities on the input parameters and Gaussian distribution of data error, there exists an analytical solution to the posterior probability of a set of input parameters $P(\mathbf{m}\,|\,\mathbf{d}_{\text{obs}})$, equal to

$$P(\mathbf{m}\,|\,\mathbf{d}_{\text{obs}}) \propto e^{-S(\mathbf{m})}, \tag{8}$$

where

$$\begin{aligned} 2S(\mathbf{m}) = {} & (\mathbf{G}\mathbf{m} - \mathbf{d}_{\text{obs}})^T \mathbf{C}_D^{-1} (\mathbf{G}\mathbf{m} - \mathbf{d}_{\text{obs}}) \\ & + (\mathbf{m} - \mathbf{m}_{\text{prior}})^T \mathbf{C}_M^{-1} (\mathbf{m} - \mathbf{m}_{\text{prior}}). \end{aligned} \tag{9}$$

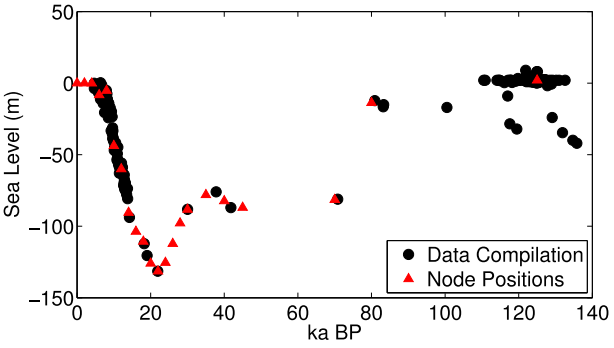

FIG. 2. Reconstructions of past sea level relative to present (black circles) and the points we use for sea level in computing the prior mean salinity and δ^{18}O (red triangles). See also Table 1.

The vector $\mathbf{d}_{\text{obs}}$ denotes the observations, $\mathbf{C}_D$ is the error covariance matrix for the data in $\mathbf{d}_{\text{obs}}$, and $\mathbf{C}_M$ is the prior error covariance matrix for the parameters in $\mathbf{m}$ (Tarantola 2005).

e. *Bayesian estimation for nonlinear problem or non-Gaussian prior parameters: Bayesian MCMC parameter estimation*

For more general cases, either nonlinear problems or when we consider parameters with arbitrary prior probability distributions, we could determine the posterior probability distribution with a grid-search approach. In such an approach, we would construct an n-dimensional grid of parameter values (n is the dimension of $\mathbf{m}$, the number of unknown parameters), with the ranges of each grid dimension determined by the prior probability distribution $P(\mathbf{m})$ of each parameter. Each point on the grid would represent a vector set of choices for $\mathbf{m}$. The initial spacing of the grid would be arbitrarily coarse and we would run the forward model at every grid point and then refine the grid spacing until the estimate of $P(\mathbf{m}\,|\,\mathbf{d}_{\text{obs}})$ converges. Our inverse problem is high dimensional (22–23 parameters), so that a grid-search approach is intractable [because of the curse of dimensionality (Bellman 1957)]. In a Bayesian MCMC approach, instead of directly computing the multidimensional integral of the probability distribution for each parameter, we build an ensemble of inverse solutions whose density in model space is proportional to the Bayesian posterior $P(\mathbf{m}\,|\,\mathbf{d}_{\text{obs}})$. For this search, we use CATMIP (Minson et al. 2013), which behaves efficiently for high-dimensional problems. CATMIP is initialized with the prior probability distribution and evolves from the prior to the posterior in a series of "tempering" or "cooling" steps. At each cooling step the algorithm recovers an intermediate probability distribution between the prior and posterior distributions. For a given set of parameter values $\mathbf{m}$, the likelihood $P(\mathbf{d}_{\text{obs}}\,|\,\mathbf{m})$ is computed by evaluating the

TABLE 1. Sea level compilation.

Age (yr)	Error (yr)	Height (m)	Error (m)	Reference	Sample core location
4674	40	−0.1	0.3	Collins et al. (1993b)	Suomi
4700	40	−3.7	0.2	Collins et al. (1993a)	Disappointment Island
5804	75	−6.6	0.5	Collins et al. (1993b)	Suomi
6368	37	−11.2	0.2	Collins et al. (1993b)	Suomi
6390	35	0.3	0.1	Collins et al. (1993b)	Morley
6716	56	−1.3	0.2	Collins et al. (1993b)	Morley
7102	82	−14.2	0.1	Collins et al. (1993b)	Suomi
7460	80	−20.5	—	Bard et al. (1990a,b)	RGF7-4-2
7962	76	−5.1	0.5	Collins et al. (1993b)	Morley
8124	44	−7.5	0.1	Collins et al. (1993b)	Morley
8160	100	−11	1	Ludwig et al. (1996)	FL-32
8191	113	−11	0.5	Collins et al. (1993b)	Morley
8363	71	−13.1	—	Edwards et al. (1993)	
8450	50	−21.9	—	Bard et al. (1990a,b)	RGF7-5-5
8520	28	−24.2	—	Bard et al. (1996)	Tahiti
8621	48	−14.1	0.4	Collins et al. (1993b)	Morley
8760	51	−20.5	—	Edwards et al. (1993)	
9000	171	−17.1	0	Collins et al. (1993b)	Morley
9245	40	−33.3	—	Bard et al. (1996)	Tahiti
9347	70	−19.8	0.2	Collins et al. (1993b)	Morley
9534	?	−23.5	0.2	Collins et al. (1993b)	Morley
9596	21	−35.6	—	Bard et al. (1996)	Tahiti
9642	72	−31.2	—	Edwards et al. (1993)	
9700	205	−38.9	—	Bard et al. (1996)	Tahiti
9730	50	−33.3	—	Bard et al. (1990a,b)	RGF7-16-2
9831	31	−38.3	—	Bard et al. (1996)	Tahiti
9920	40	−40.6	—	Bard et al. (1996)	Tahiti
10 113	42	−47.0	—	Bard et al. (1996)	Tahiti
10 201	31	−45.0	—	Bard et al. (1996)	Tahiti
10 250	40	−45.1	—	Bard et al. (1996)	Tahiti
10 490	77	−41.6	—	Edwards et al. (1993)	
10 575	50	−47.9	—	Bard et al. (1996)	Tahiti
10 673	25	−45.6	—	Edwards et al. (1993)	
10 850	50	−53.8	—	Bard et al. (1996)	Tahiti
10 912	27	−52.7	—	Edwards et al. (1993)	
10 955	54	−49.3	—	Edwards et al. (1993)	
11 004	14	−53.9	—	Bard et al. (1996)	Tahiti
11 045	57	−53.4	—	Edwards et al. (1993)	
11 090	70	−44.8	—	Bard et al. (1990a,b)	RGF7-27-4
11 280	30	−56.9	—	Bard et al. (1996)	Tahiti
11 495	30	−62.9	—	Bard et al. (1996)	Tahiti
11 530	70	−58.9	—	Bard et al. (1990a,b)	RGF12-5-2
11 590	60	−56.9	—	Bard et al. (1990a,b)	RGF12-6-7
11 930	50	−63.1	—	Bard et al. (1996)	Tahiti
12 084	70	−55.9	—	Edwards et al. (1993)	
12 155	56	−58.1	—	Edwards et al. (1993)	
12 260	90	−62.2	—	Bard et al. (1990a,b)	RGF12-9-5
12 332	39	−58.9	—	Edwards et al. (1993)	
12 695	60	−71.1	—	Bard et al. (1996)	Tahiti
12 710	50	−71.8	—	Bard et al. (1996)	Tahiti
12 800	30	−69.5	—	Bard et al. (1996)	Tahiti
12 818	37	−64.1	—	Edwards et al. (1993)	
12 837	68	−67.2	—	Edwards et al. (1993)	
12 865	50	−72.2	—	Bard et al. (1996)	Tahiti
12 875	40	−69.5	—	Bard et al. (1996)	Tahiti
12 905	50	−73.7	—	Bard et al. (1996)	Tahiti
13 065	30	−74.8	—	Bard et al. (1996)	Tahiti
13 106	81	−69.5	—	Bard et al. (1990a,b)	RGF12-16-5 #1,2
13 129	84	−70.4	—	Edwards et al. (1993)	

TABLE 1. (*Continued*)

Age (yr)	Error (yr)	Height (m)	Error (m)	Reference	Sample core location
13 465	38	−77.8	—	Bard et al. (1996)	Tahiti
13 700	170	−73.7	—	Bard et al. (1990a,b)	RGF12-21-6
13 746	31	−80.8	—	Bard et al. (1996)	Tahiti
14 230	100	−93.8	—	Bard et al. (1990a,b)	RGF9-8-2
18 240	140	−112.2	—	Bard et al. (1990a,b)	RGF9-21-11
19 030	100	−120.5	—	Bard et al. (1990a,b)	RGF9-27-5 #1,2
21 930	150	−131.5	—	Bard et al. (1990a,b)	RGF9-34-8 #1,2
30 040	210	−88.2	0	Bard et al. (1990a,b)	RGF12-30-2 #1,2
37 800	600	−76	3	Chappell et al. (1996)	BOBO-U10
41 800	1200	−87	5	Chappell et al. (1996)	KANZ-U9
70 820	600	−81.1	—	Bard et al. (1990a,b)	RGF1-17-4
80 900	1700	−12.2	1	Ludwig et al. (1996)	FL-23
83 200	900	−16.5	1	Ludwig et al. (1996)	FL-20
83 300	300	−15	3	Gallup et al. (1994)	FS-3
92 100	700	−7.9	—	Esat et al. (1999)	Kanzarua Terr. VIa
98 800	800	−12.7	—	Esat et al. (1999)	Kwambu Terr. VIa
100 500	1100	−17	—	Bard et al. (1990a,b)	AFZ-2
106 400	1000	−27.2	—	Esat et al. (1999)	Kwambu Terr. VIa
110 500	3800	2	—	Szabo et al. (1994)	
110 900	3500	2	—	Szabo et al. (1994)	
112 700	800	−65.6	—	Esat et al. (1999)	Kanzarua Terr. VIa
113 200	800	−40.1	—	Esat et al. (1999)	Kwambu Terr. VIa
114 100	1800	2	—	Szabo et al. (1994)	
114 600	2600	2	—	Szabo et al. (1994)	
114 800	2100	2	—	Szabo et al. (1994)	
115 000	900	−84	—	Esat et al. (1999)	Aladdin's Cave
115 000	1000	1.71	—	Stirling et al. (1998)	Vlaming Head
116 100	900	0.36	—	Stirling et al. (1998)	Mangrove Bay
117 000	1000	−9	3	Gallup et al. (1994)	UWI-16
117 100	1600	2	—	Collins et al. (1993a)	
117 600	1200	−28.4	—	Stein et al. (1993)	KIL-5(a-2)
117 600	1900	2	—	Szabo et al. (1994)	
117 800	1700	2	—	Szabo et al. (1994)	
118 000	2000	2	—	Szabo et al. (1994)	W. Nanda Terr. VIa
118 200	1000	0.47	—	Stirling et al. (1998)	Mangrove Bay
119 000	1800	2	—	Szabo et al. (1994)	
119 200	1000	1.35	—	Stirling et al. (1998)	Mangrove Bay
119 500	1200	−32.05	—	Stein et al. (1993)	KIL-5(a-1)
119 800	1000	3.27	—	Stirling et al. (1998)	Yardie Creek
119 900	1400	2	—	Chen et al. (1991)	1
120 300	2500	2	—	Szabo et al. (1994)	
120 400	3000	2	—	Szabo et al. (1994)	
121 100	1100	2.72	—	Stirling et al. (1998)	Yardie Creek
121 100	1200	2.44	—	Stirling et al. (1998)	Yardie Creek
121 600	1000	1.87	—	Stirling et al. (1998)	Yardie Creek
121 700	1100	3	—	Stirling et al. (1998)	
121 700	1500	2	—	Szabo et al. (1994)	Burney
121 800	800	1.67	—	Stirling et al. (1995)	Leander Point
121 900	1100	9	—	Bard et al. (1990a,b)	Haiti C-1
122 000	1500	2	—	Chen et al. (1991)	2
122 100	1400	1	—	Chen et al. (1991)	AFS-12 A
122 100	1300	1	—	Chen et al. (1991)	24
122 100	1100	6	—	Edwards et al. (1988)	34
122 200	1000	1.73	—	Stirling et al. (1998)	Burney
122 300	1000	2	—	Chen et al. (1991)	6
122 800	1600	1	—	Chen et al. (1991)	36
123 000	1000	3.04	—	Stirling et al. (1998)	Burney
123 200	2600	2	—	Szabo et al. (1994)	

TABLE 1. (*Continued*)

Age (yr)	Error (yr)	Height (m)	Error (m)	Reference	Sample core location
123 300	1500	1	—	Chen et al. (1991)	35
123 300	900	1.8	—	Stirling et al. (1995)	Leander Point
123 400	900	2.2	—	Stirling et al. (1995)	Leander Point
123 500	1100	3.09	—	Stirling et al. (1998)	Burney
123 600	1200	2	—	Chen et al. (1991)	3
123 700	800	1.28	—	Stirling et al. (1995)	Leander Point
123 800	1500	1	—	Chen et al. (1991)	32
123 800	1100	1	—	Chen et al. (1991)	37
123 800	900	0.7	—	Stirling et al. (1995)	Leander Point
124 000	2000	1.8	0.1	Collins et al. (1993a)	
124 000	1200	2	—	Szabo et al. (1994)	
124 100	1500	2.16	—	Stirling et al. (1995)	Leander Point
124 200	900	0.68	—	Stirling et al. (1995)	Leander Point
124 300	1000	1.2	—	Stirling et al. (1998)	Tantabiddi Bay
124 500	1300	6	—	Edwards et al. (1988)	C
124 700	1000	2.3	—	Stirling et al. (1998)	Yardie Creek
124 800	1100	0.92	—	Stirling et al. (1998)	Vlaming Head
124 900	1300	8	—	Bard et al. (1990a,b)	Haiti C-4 #1,2
124 900	2100	0	—	Chen et al. (1991)	29
125 000	3800	2	—	Szabo et al. (1994)	
125 100	1000	8	—	Bard et al. (1990a,b)	AFM3 #1,2
125 100	1300	2	—	Szabo et al. (1994)	
125 400	900	1.83	—	Stirling et al. (1995)	Rottnest Island
125 400	1100	0.92	—	Stirling et al. (1998)	Vlaming Head
125 400	1100	1.79	—	Stirling et al. (1998)	Mangrove Bay
125 500	800	0.45	—	Stirling et al. (1995)	Rottnest Island
125 700	900	−101.1	—	Esat et al. (1999)	Aladdin's cave
126 000	800	2.43	—	Stirling et al. (1995)	Rottnest Island
126 200	800	1.77	—	Stirling et al. (1995)	Rottnest Island
126 600	900	2.16	—	Stirling et al. (1995)	Leander Point
126 800	1000	2.37	—	Stirling et al. (1998)	
126 800	2300	2	—	Szabo et al. (1994)	Yardie Creek
127 000	2100	2	—	Szabo et al. (1994)	
127 200	1500	1	0	Chen et al. (1991)	22
127 300	1000	2.43	0	Stirling et al. (1995)	Rottnest Island
127 600	900	−104.2	—	Esat et al. (1999)	Aladdin's cave
127 800	1100	−1.79	—	Stirling et al. (1998)	Drillcore coral
127 900	1200	1	0	Chen et al. (1991)	19
128 100	900	−97.0	—	Esat et al. (1999)	Kwangam Terr. VIb
128 400	1200	0	—	Chen et al. (1991)	30
128 500	6100	2	—	Szabo et al. (1994)	
128 600	1100	0.7	—	Stirling et al. (1998)	Yardie Creek
128 900	1200	−0.69	—	Stirling et al. (1998)	Drillcore coral
129 100	800	−24	3	Gallup et al. (1994)	UWI-2
129 200	1300	2	—	Szabo et al. (1994)	
129 900	900	−107.8	—	Esat et al. (1999)	Aladdin's cave
129 900	1000	−107.8	—	Esat et al. (1999)	Aladdin's cave
129 900	900	−107.8	—	Esat et al. (1999)	Aladdin's cave
130 200	2500	2	—	Szabo et al. (1994)	
130 600	1000	−109.0	—	Esat et al. (1999)	Aladdin's cave
131 000	2700	2	—	Szabo et al. (1994)	
131 900	1200	−34.6	—	Stein et al. (1993)	HP23b
132 600	3300	2	—	Szabo et al. (1994)	
133 000	1000	−112.8	—	Esat et al. (1999)	Aladdin's cave
133 700	1000	−113.9	—	Esat et al. (1999)	Aladdin's cave
134 700	1300	−39.9	—	Stein et al. (1993)	HP-23a
135 800	1900	−42.	—	Stein et al. (1993)	HP-22
136 700	1600	−32.7	—	Esat et al. (1999)	Sialum Terr. VIIb

forward model and computing a misfit cost function between the model prediction and the measured data.

f. Parameterization of inverse problem

In practice, we must solve for a discrete rather than continuous set of variables. We therefore frame our inverse problem, the solution for a time series from a vertical concentration profile, as a set of discrete parameters. We are primarily interested in recovering the bottom water history, the time series of $[Cl^-]$ or $\delta^{18}O$ at the ocean floor, but its solution is not independent of the other unknowns. As we show later (see section 7), the solution is particularly sensitive to D_0'; therefore, we seek to simultaneously recover the bottom water history and the coefficient D_0'. The bottom water history is parameterized as salinity at 22 unevenly spaced, fixed time points, which we henceforth refer to as nodes. The nodes are spaced 2000 years apart near the present-day, with coarser resolution further back in time to 125 000 years BP. The number of nodes is consistent with the observation that only $O(10)$ nodes can be resolved by the data [nodes arranged at fixed points in time, determined by examination of the singular value decomposition (SVD) of the discrete Green's functions generated from the 1D advection–diffusion equation (Miller 2014)]. Higher temporal resolution of the parameterization increases the computational expense of the fully nonlinear inverse problem without a qualitative change in the inverse solution set. To retain accuracy in the forward finite difference solver, we linearly interpolate between the parameters at fixed times to generate the input to the forward model.

g. Likelihood function

We assume our error has a Laplace (or double exponential) distribution to compute the likelihood function

$$P(\mathbf{d}_{\text{obs}}\,|\,\mathbf{m}) \propto \exp\left(-\frac{1}{2}\{[\mathbf{G}(\mathbf{m})-\mathbf{d}_{\text{obs}}]^T\mathbf{C}_D^{-1}[\mathbf{G}(\mathbf{m})-\mathbf{d}_{\text{obs}}]\}^{1/2}\right). \tag{10}$$

The data covariance matrix $\mathbf{C}_D$ has only diagonal terms σ^2, where σ is one standard deviation of the measurement error.

We use a Laplace error distribution rather than the commonly used Gaussian error distribution in order to reduce the effect of data outliers on our solutions. Note that in general the form of the Laplace distribution is $\propto \exp[-(|x-\mu|/b)]$, while the Gaussian distribution is $\propto \exp\{-[(x-\mu)^2/2\sigma^2]\}$. To maintain roughly the same nominal probability within two standard deviations of the mean, we assign $b = 2\sigma$.

3. The prior probability of the bottom water history $P(\mathbf{m})$

We represent our prior knowledge of the salinity or $\delta^{18}O$ bottom water histories as multidimensional Gaussian distributions. The value of salinity or $\delta^{18}O$ at each fixed time point in the discrete bottom water history is a parameter in our problem. We assign a prior mean and variance to each node. The mean represents our estimate of the global deep ocean mean, while the variance represents our best guess of the global spread of deep ocean salinities or $\delta^{18}O$ values around the mean at that time. To ensure smoothly varying solutions, we further impose temporal covariance between node values.

a. Prior information from sea level records

There is little information about spatial or temporal variations in past deep ocean salinity from paleo proxies. However, sea level reconstructions give us a useful prior estimate of the mean ocean salinity. Assuming the major ions in seawater are conservative over our time period of interest, the mean ocean salinity is proportional to the volume of water in the oceans, itself proportional to sea level. We treat the ocean as a rectangular basin that is 3800 m deep today and 131.5 m lower at the LGM (Bard et al. 1990a,b) so that the concentrations scale directly to changes in sea level as

$$\mu_S(t) = \mu_S|_{\text{mod}} + \frac{h(t)-h_{\text{mod}}}{h_{\text{LGM}}-h_{\text{mod}}}(\mu_S|_{\text{LGM}} - \mu_S|_{\text{mod}}). \tag{11}$$

Here mod indicates the modern mean ocean value and h is the mean ocean depth. For consistency with the assumptions made in Adkins et al. (2002), we take the modern mean ocean salinity to be $34.68\,\text{g}\,\text{kg}^{-1}$ and the LGM mean ocean salinity to be $\mu_S|_{\text{LGM}} = h_{\text{mod}}\mu_S|_{\text{mod}}/h_{\text{LGM}} = 35.9\,\text{g}\,\text{kg}^{-1}$. Our sea level curve is interpolated from a new compilation of published values (Fig. 2, Table 1).

Conversion from total ice mass to the mean $\delta^{18}O_w$ of the ocean requires knowledge of the spatial and temporal variability of $\delta^{18}O$ of mountain glaciers and continental ice sheets. Estimates of these variations of $\delta^{18}O$ in the past are relatively unconstrained by measurements, making it impossible to quantify their associated errors. There are many existing estimates of the past contribution of $\delta^{18}O|_w$ ($\delta^{18}O$ of water) to the $\delta^{18}O|_c$ ($\delta^{18}O$ of carbonate) of benthic foraminifera at the LGM (e.g., Emiliani 1966; Shackleton 1967; Dansgaard and Tauber 1969; Chappell and Shackleton 1986; Fairbanks 1989; Mix 1987; Schrag et al. 1996). Duplessy et al. (2002) reviews the traditional ice-mass-based estimates of $\delta^{18}O$ at the LGM and suggests a lower bound of ocean mean $\delta^{18}O|_w$ of 0.85‰

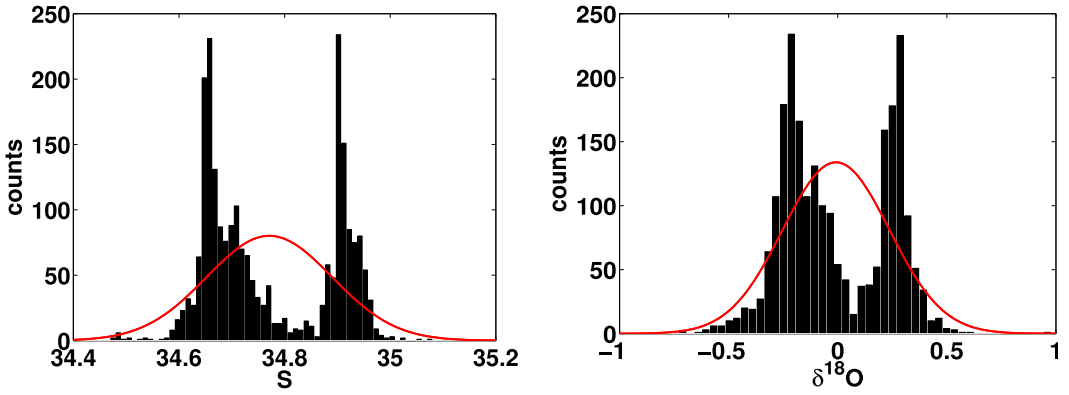

FIG. 3. Modern deep ocean measurements below 2000 m, excluding the Mediterranean Sea from the GISS Global Seawater Oxygen-18 gridded database (Schmidt et al. 1999; LeGrande and Schmidt 2006). Red curves are Gaussian distribution fits to data. (a) Modern S below 2000 m and (b) modern δ^{18}O below 2000 m.

based on the freezing point of seawater and an upper bound based on ice mass approximations of 1.47‰. We take the best current guess of the LGM mean ocean δ^{18}O to be the midpoint of the Duplessy et al. (2002) ice mass bounds, 1.16‰. The equation for deep ocean δ^{18}O as a function of time (sea level) is similar to that of $\mu_S(t)$ [Eq. (11)], with modern mean $\delta^{18}\mathrm{O} = 0$.

b. *Prior information from modern ocean property spatial spreads*

Today, salinities and δ^{18}O everywhere in the deep ocean are close to their mean ocean value. Distributions of δ^{18}O and salinity in the past are unknown. Lacking other constraints, we might guess that past spatial distributions of deep δ^{18}O and salinity around their mean ocean values were the same as their modern spatial distributions. The full ocean modern distributions of salinity and δ^{18}O deeper than 2000 m (LeGrande and Schmidt 2006) are not simple Gaussians (Fig. 3); at best they are a mixture of Gaussians. The bimodal nature of the modern distributions comes from the dominance in the modern deep ocean of North Atlantic Deep Water and Antarctic Bottom Water, two water masses with distinct properties. However, the modern ranges of salinity and δ^{18}O at a given site are narrow. The bimodality of the global distributions of salinity and δ^{18}O are due primarily to spatial rather than temporal (e.g., seasonal, interannual) variability.

In the vicinity of each site on the ocean floor, the modern distribution of salinity and δ^{18}O could be described by a Gaussian. However, we wish to avoid imposing the modern ocean state on the glacial ocean state by assuming, for example, that salinity is high in the North Atlantic and low in the Southern Ocean. A less stringent prior assumption is that the feasible end-to-end ranges of salinity and δ^{18}O at any site in the past match the modern deep ocean end-to-end ranges. As a conservative estimate for the modern spread of salinity and δ^{18}O, we fit a Gaussian probability distribution envelope around each histogram, as shown by the red curves in Fig. 3. Applying this method gives a modern deep ocean standard deviation of salinity of $\sigma_S = 0.12\,\mathrm{g\,kg^{-1}}$ and a standard deviation of δ^{18}O of $\sigma_{\delta^{18}O} = 0.25$‰. In addition to the possible values for deep ocean properties, the prior variances must also account for error in the sea level curve. An error of 10 m in height propagated through the scaling for sea level gives an error ϵ_{μ_s} of $0.093\,\mathrm{g\,kg^{-1}}$ in salinity, assuming the LGM height and salinity are known. The error propagation formula is $\epsilon_{\mu_s} = \sqrt{(\partial\mu_s/\partial h)^2(\delta h)^2}$, with $\delta h = 10$ m and $\partial\mu_s/\partial h = (\mu_s|_{\mathrm{LGM}} - \mu_s|_{\mathrm{mod}})/(h_{\mathrm{LGM}} - h_{\mathrm{mod}})$. The error in δ^{18}O is not directly related to the sea level; however, Duplessy et al. (2002) suggest an error in their estimate for mean $\delta^{18}\mathrm{O}_w$ should be 0.2‰. Summing together the modern variance and the estimated error in sea level yields $\sigma_S = 0.213\,\mathrm{g\,kg^{-1}}$ ($\sigma_S^2 = 0.05\,\mathrm{g^2\,kg^{-2}}$) and $\sigma_{\delta^{18}O} = 0.45$‰ [$\sigma^2_{\delta^{18}O} = 0.20(‰)^2$].

c. *Prior information about ocean property temporal variations*

As neighboring points in a time series at a given location are not independent, we assign covariances to the points in the time series. We adopt covariances with the form

$$\sigma_{ij} = \sigma_{ii}^2 \exp\left[-\frac{(t_i - t_j)^2}{2T^2}\right], \tag{12}$$

where T is a time scale of covariance and i and j are matrix indices denoting discrete values of the parameterized time series. When $t_i - t_j = T$, the correlation between the time series values at those times is

$\sim$0.6, while if $t_i - t_j = 2T$, the correlation between the values is $\sim$0.1.

The covariance time scale T represents roughly half of an ocean site's memory of its previous salinity or δ^{18}O value. Time scale T is a spatially variable function of ocean mixing, which will also depend on the global distribution of temperature and salinity (through density). Assuming that large-scale steady-state ocean tracer mixing is a balance between advection and eddy diffusion, that is, as in Ferrari and Wunsch (2009),

$$\mathbf{v} \cdot \nabla C = \nabla \cdot (\mathbf{K} \nabla C), \tag{13}$$

where $\mathbf{v}$ is the fluid velocity; C is the tracer concentration field; and $\mathbf{K}$ is the (eddy) diffusivity of a tracer, in general a spatially variable tensor. We can scale Eq. (13) to relate the time scale T to an eddy diffusivity κ using a characteristic length scale L. That is,

$$2T \propto \frac{L^2}{\kappa}, \tag{14}$$

where $2T$ is the time needed for an ocean site to forget its previous value. Assuming that mixing predominantly proceeds along isopycnals, recent estimates suggest κ is $O(100)\,\mathrm{m^2\,s^{-1}}$ (Zika et al. 2009, 2010). For deep ocean sites under the influence of spatially homogeneous deep water masses, we assume L is at least half the meridional extent of the Atlantic Ocean, roughly 8000 km. With these values for L and κ, T is $\sim$10 000 years.

Our scaling argument assumes a steady-state ocean circulation and is simplistic. Paleoceanographic records suggest that the ocean does not remain in steady state over $O(10^4)$ years (e.g., Charles et al. 1996; Hodell et al. 2003; Lamy et al. 2004; Lynch-Stieglitz 2004; Pahnke and Zahn 2005; Robinson et al. 2005). Using radiocarbon ages to estimate the reservoir age of the deep ocean, some authors conclude that the ocean can reach a new steady state after 2000 years (Duplessy et al. 1991; Skinner and Shackleton 2005), implying that $T = 1000$ years. However, Wunsch and Heimbach (2008) demonstrate that radiocarbon ages can be misleading; the ocean may need up to 10 000 years to reach a new equilibrium in response to regional changes in surface forcing. In our framework this is equivalent to $T = 5000$ years or more.

d. *Accounting for different-than-modern past ocean property spreads*

Adkins et al. (2002) conclude that the spread in LGM deep ocean salinity was larger than it is today. Their results demonstrate that the measurements are consistent with a larger-than-modern spread in salinity, but they do not require that the salinity spread was so large. It is possible that the ocean had a wider salinity spread in the past, but we do not have any a priori information on what the magnitude of the spread was.

Bayesian methods allow us to shrink but not expand the distribution on any given parameter. With an assumed Gaussian prior, posterior estimates more than two standard deviations from the mean of the prior are unlikely, as any parameters with 0 prior probability will, by definition, have 0 posterior probability [recall that $P(\mathbf{m}\,|\,\mathbf{d}_{\mathrm{obs}}) \propto P(\mathbf{d}_{\mathrm{obs}}\,|\,\mathbf{m})P(\mathbf{m})$, so $P(\mathbf{m}) = 0$ implies that $P(\mathbf{m}\,|\,\mathbf{d}_{\mathrm{obs}}) = 0$]. To allow for the possibility of the LGM salinities estimated by Adkins et al. (2002), we consider the sensitivity of our solution to wider-than-modern prior variances, in particular a prior variance equivalent to that implied by the spread in Adkins et al. (2002), $\sigma_S^2 = 0.5\,\mathrm{g^2\,kg^{-2}}$.

e. *Diffusion coefficient prior*

We assign a lognormal prior to the diffusion coefficient D_0' because D_0' is a Jeffreys parameter. Jeffreys parameters are physical parameters that are always positive but could vary by orders of magnitude (Tarantola 2005). Laboratory studies find values of D_0 for chloride between 1×10^{-6} and $20 \times 10^{-6}\,\mathrm{cm^2\,s^{-1}}$, varying as a function of temperature, pressure, and ionic content (Li and Gregory 1974). The D_0 of δ^{18}O is the relative diffusivity of water oxygen isotopes, which mirrors the diffusivity of $H_2^{18}O$ in water, $O(1 \times 10^{-5})\,\mathrm{cm^2\,s^{-1}}$, also a function of temperature (Wang et al. 1953). In our nonlinear inversions in which we estimate D_0', we choose a prior mean diffusion coefficient of $5.05 \times 10^{-5}\,\mathrm{cm^2\,s^{-1}}$ and the standard deviation of the $\ln(D_0')$ equal to 1.5, as shown in Fig. 4.

4. Synthetic example framework

We consider several synthetic problems to examine the extent to which we can recover bottom water salinity histories from pore fluid profiles. The details of each synthetic example vary, but all follow the same basic approach. We choose hypothetical bottom water salinity histories, which we refer to as $S_{\mathrm{BW}}(t)$. Using a known $S_{\mathrm{BW}}(t)$ as the top (ocean–sediment interface) boundary condition in the forward problem (see section 2a), we generate synthetic data: an ocean sediment pore fluid salinity profile. Random synthetic Gaussian noise of 0.05% is added to the synthetic data to represent measurement uncertainties. We then use CATMIP to invert the noisy synthetic data and recover a posterior distribution of $S_{\mathrm{BW}}(t)$, which we compare to the known $S_{\mathrm{BW}}(t)$ to determine how well we can recover the true solution by inverting the data. The difference between the posterior (inverse) estimate and the true $S_{\mathrm{BW}}(t)$ is

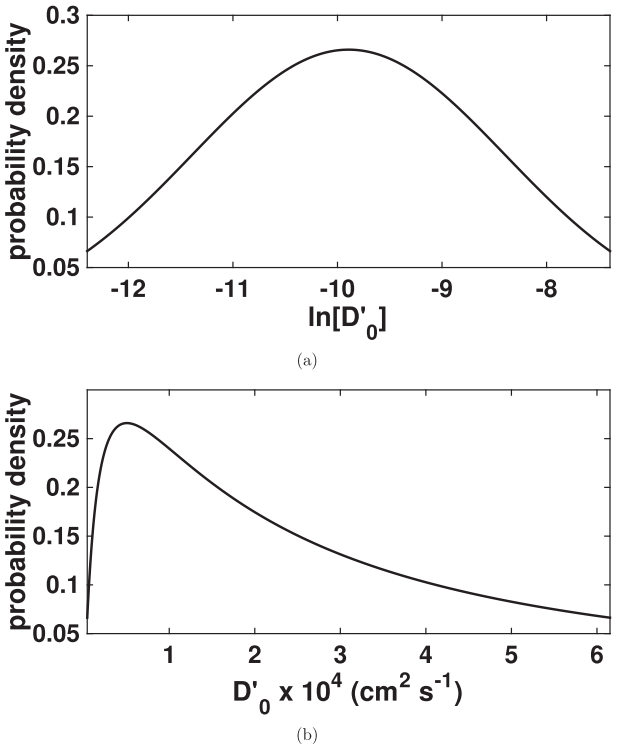

FIG. 4. Prior distribution for D_0' is lognormal centered on $5.05 \times 10^{-5}\,\mathrm{cm^2\,s^{-1}}$, with standard deviation of the natural logarithm equal to 1.5. (a) Prior probability density plotted as a function of the natural logarithm of D_0'. (b) Prior probability density plotted as a function of D_0'.

summarized by the root-mean-square difference $\epsilon = (1/\sqrt{N})\{\sum_{i=1}^{N}[S_{\mathrm{BW}}(t_i)|_{\mathrm{post}} - S_{\mathrm{BW}}(t_i)|_{\mathrm{true}}]^2\}^{1/2}$ in each figure caption. The experiments are summarized in Table 2.

5. Linear problem: Inversion for bottom water salinity history, $S_{\mathrm{BW}}(t)$ only

a. *Inversion of synthetic stretched sea level example with varying prior assumptions*

Our first example is modeled after Adkins et al.'s (2002) reconstructed bottom water salinity history in the Southern Ocean (ODP site 1093), the location with highest inferred salinity at the LGM. We suppose that this was the true bottom water history in order to determine what information about such a history would be retained by the modern measured pore fluid profile. To construct $S_{\mathrm{BW}}(t)$, we start with a presumed mean ocean salinity history, $\mu_S(t)$ (see section 3a). We multiply $\mu_S(t)$ by a constant factor, determined by assuming that the LGM salinity in the Southern Ocean was $37.1\,\mathrm{g\,kg^{-1}}$ [as inferred by Adkins et al. (2002)]. We call this synthetic $S_{\mathrm{BW}}(t)$ as the "stretched sea level" example. The diffusivity parameter D_0' is $2.5 \times 10^{-5}\,\mathrm{cm^2\,s^{-1}}$, and r and dr/dz are computed from the temperature profile at ODP site 1093 (Gersonde et al. 1999). The variable u_H is $0.01\,\mathrm{cm\,yr^{-1}}$, and the model domain (sedimentary column) is 350-m long. The initial salinity profile is interpolated from the measured chlorinity profile (converted to salinity) at ODP site 1093, as in Adkins et al. (2002). Here we assume that the cyclical nature of glaciations and deglaciations would have caused the depth profile of $[\mathrm{Cl^-}]$ to be the same at the last interglacial (125 000 yr BP) as it is today. The bottom boundary condition is $(\partial C/\partial z)|_{z=350\,\mathrm{m}} = 0$.

For the purpose of our present work, we assume that the mean ocean salinity history $\mu_S(t)$ is known up to an error of $0.093\,\mathrm{g\,kg^{-1}}$ (see section 3b). Deep ocean salinities should be near the mean ocean value; however, we do not have any prior information on the variance of salinity at the LGM. The range in deep ocean salinities at the LGM reported in Adkins et al. (2002) corresponds to a variance of approximately $\sigma_S^2 = 0.5\,\mathrm{g^2\,kg^{-2}}$, while a generous estimate of deep ocean salinity variability from existing modern compiled measurements combined with LGM sea level error is $\sigma_S^2 \approx 0.05\,\mathrm{g^2\,kg^{-2}}$. The full range of modern ocean salinity is encompassed by a variance $\sigma_S^2 = 100\,\mathrm{g^2\,kg^{-2}}$ (one standard deviation range is ~25–45 $\mathrm{g\,kg^{-1}}$). Similarly, we expect temporal correlation in $S_{\mathrm{BW}}(t)$, but we also have few constraints on the value of the correlation time scale T. As discussed in section 3, T could be as short as a few hundred years or it could be greater than 5000 years.

With these points in mind, we invert the synthetic data assuming prior variances $\sigma_S^2 = 0.05, 0.5$, and $100\,\mathrm{g^2\,kg^{-2}}$. As

TABLE 2. Summary of experiments.

	Prior distribution		
Synthetic $S_{\mathrm{BW}}(t)$	$\mu_S(t)$	σ_S^2 ($\mathrm{g^2\,kg^{-2}}$)	T (yr)
Stretched sea level	Scaled sea level (see section 3a)	100	0–6000
		0.5	0–4000
		0.05	0–4000
Random time series (×10)	Scaled sea level (see section 3a)	100	0–6000
		0.5	0–4000
		0.05	0–4000

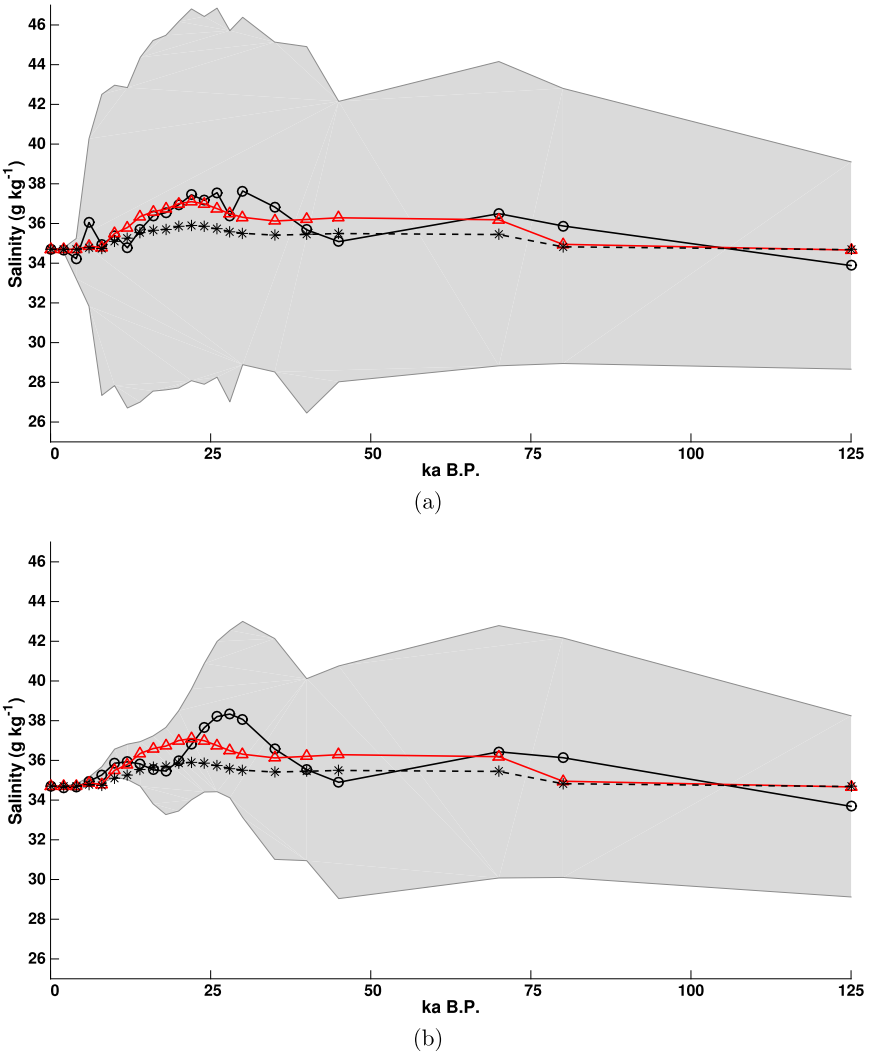

FIG. 5. Linear stretched sea level synthetic example with uninformative prior variance $\sigma_S^2 = 100\,\mathrm{g}^2\,\mathrm{kg}^{-2}$. Red line with triangular markers is the known synthetic $S_{\mathrm{BW}}(t)$. The black open circles are the mean posterior values of $S_{\mathrm{BW}}(t)$ (i.e., the salinity values estimated by inversion). Gray shading denotes the standard deviation of the posterior distribution. Black dashed line with star markers is the prior mean. (a) Case where no temporal covariance in bottom water salinity is assumed ($T = 0$ years), $\epsilon = 0.66$. (b) Case with a covariance time scale $T = 6000$ years, $\epsilon = 0.92$.

shorthand, we refer to these as "modern," "intermediate," and "uninformative" variances, respectively. We also vary the prior assumed covariance time scale T and consider its effect on the posterior distribution of $S_{\mathrm{BW}}(t)$.

The results of the uninformative prior variance example, $\sigma_S^2 = 100\,\mathrm{g}^2\,\mathrm{kg}^{-2}$, illustrate that the measured data constrain the absolute values of salinity between 6 ka BP and present when T is assumed to be 0 years (Fig. 5). Note that even when T is assumed to be 0 years, there is some temporal correlation implicit in $\mu_S(t)$. By increasing the value of T while holding σ_S^2 constant, we find that the posterior variance of $S_{\mathrm{BW}}(t)$ is a strong function of T. Increasing T decreases the posterior variance of $S_{\mathrm{BW}}(t)$, particularly between ~26 ka BP and the present (Fig. 6). However, a reduction of the posterior variance relative to the prior variance of $S_{\mathrm{BW}}(t)$ does not guarantee that the mean posterior estimate aligns with the true solution, as demonstrated in Fig. 5.

As shown in Fig. 5, the mean posterior estimate of $S_{\mathrm{BW}}(t)$ (here equivalent to the mode or highest-probability inverse solution) oscillates around the true synthetic $S_{\mathrm{BW}}(t)$ at times that have a wide posterior variance. This oscillation suggests that while the data do not constrain the value of salinity at these times, they do constrain temporal correlations in $S_{\mathrm{BW}}(t)$, that is, the relative value of salinities at different times in the bottom water history. For this

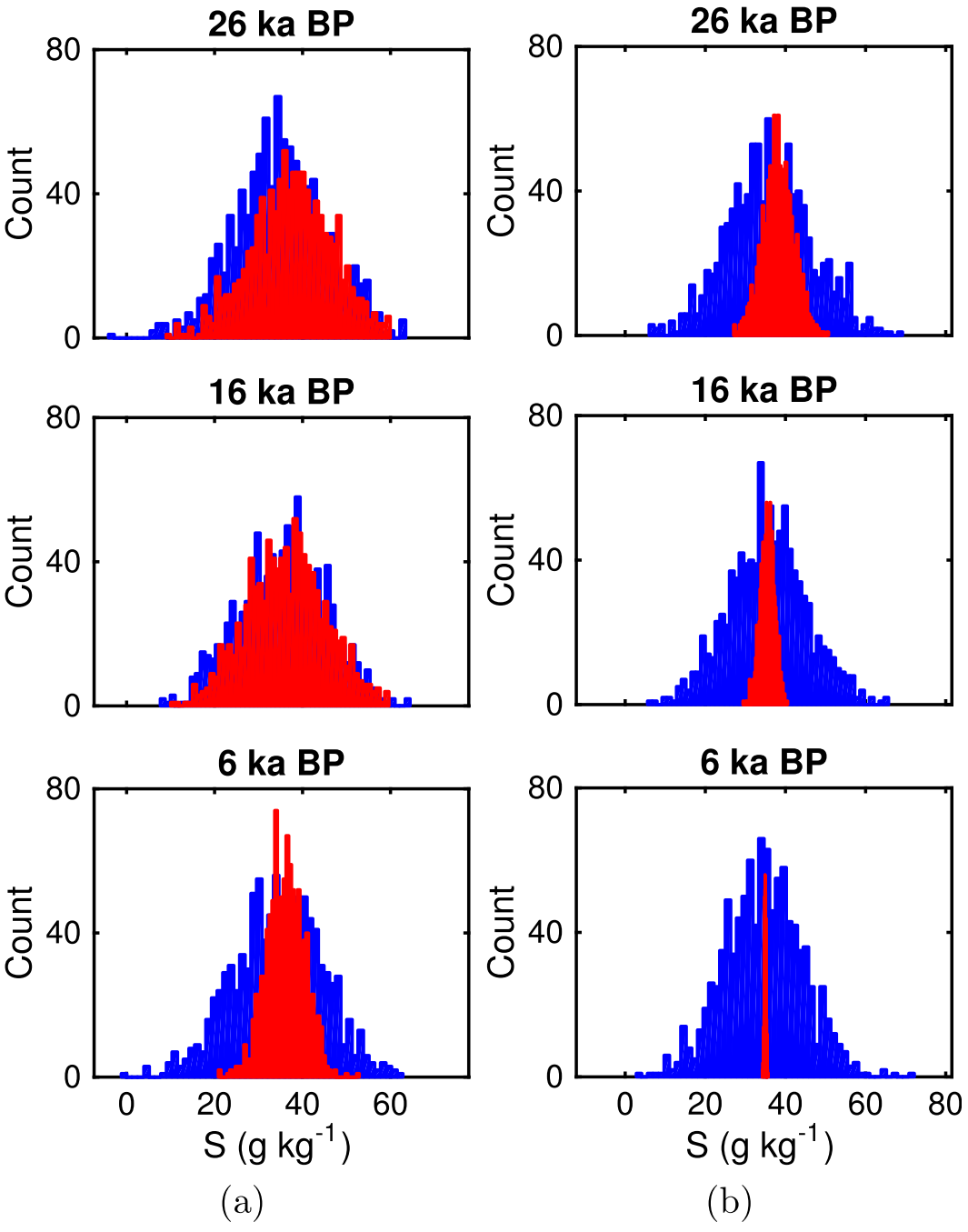

FIG. 6. Histograms of the prior (blue) and posterior (red) distributions of bottom water salinity. Histograms are directly proportional to the marginal distributions of each variable (i.e., the absolute probability of the variable not conditioned on any other variable). The prior distribution is characterized by a variance $\sigma_S^2 = 100\,\mathrm{g}^2\,\mathrm{kg}^{-2}$. (a) Case where no temporal covariance in bottom water salinity is assumed ($T = 0$ years), $\epsilon = 0.66$ (b) Case with a covariance time scale $T = 6000$ years, $\epsilon = 0.92$.

reason we compare the frequency content of the prior and posterior estimates (Fig. 7). The frequency content of the prior $\mu_S(t)$ is set equal to the frequency content of the true synthetic stretched sea level $S_{\mathrm{BW}}(t)$, so it is unsurprising that the frequency content of the posterior estimates are similar to the frequency content of the true $S_{\mathrm{BW}}(t)$. Imposing nonzero values of T does filter the frequency content of the posterior estimate, removing power at the upper and lower ends of the frequency range. In this particular example, the data do not constrain the frequency

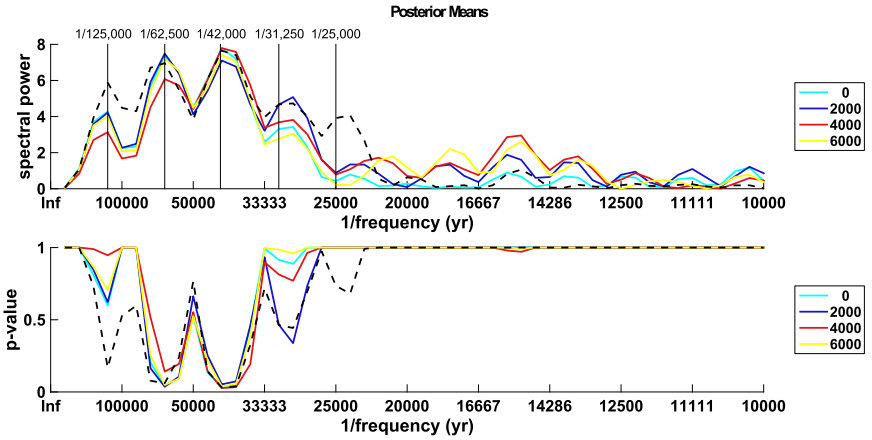

FIG. 7. Lomb–Scargle periodogram of the posterior mean $S_{BW}(t)$ for the stretched sea level example using a Gaussian prior with variance $100\,g^2\,kg^{-2}$. Spectral power units are variance of the time series ($g^2\,kg^{-2}$). The p value is the probability (at the 99% significance level) that the power detected at a given frequency is generated by N independent random Gaussian variables (noise), where N is the number of frequencies sampled in computing the periodogram. The black dashed line is the periodogram of the prior mean that is equivalent to the periodogram of the true synthetic $S_{BW}(t)$. Each color is the periodogram of the posterior mean with a different prior covariance time scale T, from 0 to 6000 years. The vertical lines overlain show the peak frequencies for the prior and those of the posterior for the example $T = 6000$ years.

content of the bottom water salinity history separately from the prior assumptions.

Assuming $\sigma_S^2 = 0.05\,g^2\,kg^{-2}$ and $T = 0$ years in the prior distribution, the synthetic $S_{BW}(t)$ falls outside one standard deviation of the posterior distribution (Fig. 8). Recall that the synthetic $S_{BW}(t)$ in this example is inconsistent with the modern prior variance assumption, because it is modeled after the high-salinity Southern Ocean case in Adkins et al. (2002). Increasing the prior variance assumption from 0.05 to $0.5\,g^2\,kg^{-2}$, holding T constant at 0 years, widens the posterior variance but does not significantly alter the mean posterior time series (cf. Fig. 9a to Fig. 8a).

Increasing the prior covariance time scale T from 0 to 4000 years improves the match of the posterior mean estimate $S_{BW}(t)$ to the true synthetic $S_{BW}(t)$ over the time period between 40 ka BP and present (Figs. 8b, 9b). The improved match of the posterior mean estimate of $S_{BW}(t)$ to the true synthetic $S_{BW}(t)$ when $T = 4000$ years results from the underlying temporal correlation of the synthetic $S_{BW}(t)$ (see Fig. 7). As expected, a more accurate prior guess leads to a more accurate posterior estimate.

b. *Inversion for random time series consistent with the Gaussian prior assumption*

In section 5a we found that our ability to recover $S_{BW}(t)$ from the modern pore fluid profile decreases with time in the past. We also showed that prior assumptions more consistent with the true synthetic $S_{BW}(t)$ led to more accurate posterior estimates. However, the prior assumptions in section 5a were not strictly consistent with the known $S_{BW}(t)$. Specifically, some values of the synthetic $S_{BW}(t)$ were outside the range prescribed by the prior variances. The term $S_{BW}(t)$ had the same frequency content as the prior $\mu_S(t)$, but the prior distribution had an additional constraint of a covariance time scale T. As shown in section 5a, the prior constraint T reduces the frequency content of the posterior mean estimate relative to the frequency content of the prior mean guess and the true $S_{BW}(t)$. For this reason, the posterior estimate may be dominated by frequencies or harmonics consistent with the prior covariance time scale, and an accurate estimate of tracer variability at one frequency may trade off with the fit to another, such that parts of the inverse estimate (e.g., millennial variability, centennial variability) are closer to the true synthetic than others.

Because the prior constraints are parameters of a multivariate Gaussian distribution, complete consistency between prior assumptions and a synthetic example requires considering a distribution of synthetic examples. We therefore construct examples in which we randomly draw an ensemble of 10 synthetic $S_{BW}(t)$ from a multivariable Gaussian distribution consistent with (equivalent to) the prior distribution. In these examples, the mean of the Gaussian is equal to $\mu_S(t)$, and we show representative cases for two different variances, $\sigma_S^2 = 0.05$ and $0.5\,g^2\,kg^{-2}$, permuted with two different covariance time scales, $T = 0$ and 4000 years. We show that even when the synthetic time series are completely consistent with the prior distribution, the

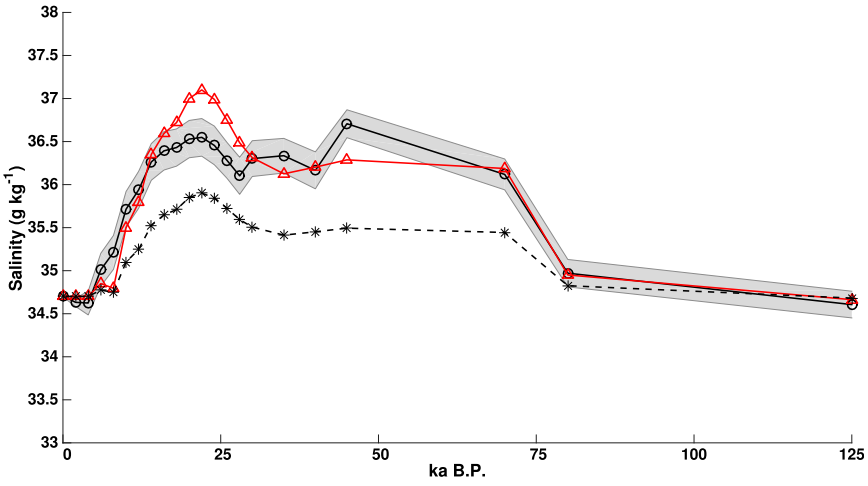

(a)

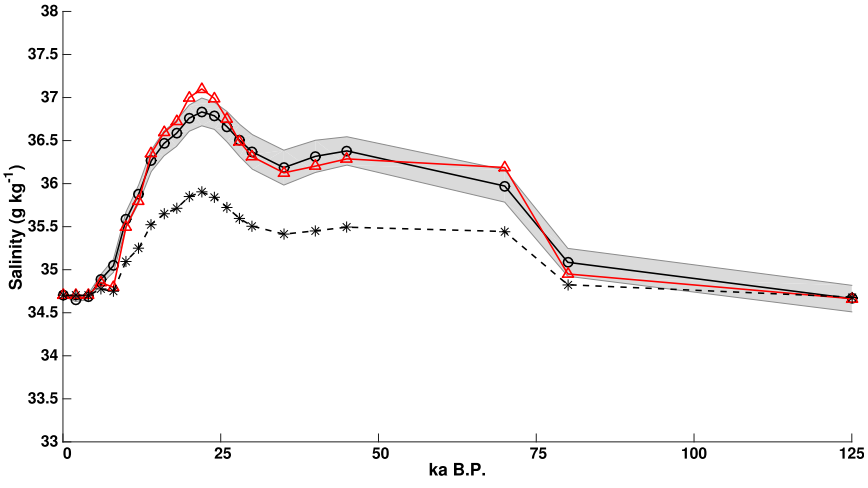

(b)

FIG. 8. Linear stretched sea level synthetic example with modern prior variance (σ_S^2 = 0.05 g^2 kg^{-2}). Red line with triangular markers is the known synthetic $S_{BW}(t)$. The black open circles are the mean posterior values of $S_{BW}(t)$ (i.e., the salinity values estimated by inversion). Gray shading denotes the standard deviation of the posterior distribution. Black dashed line with star markers is the prior mean. (a) Case where no temporal covariance in bottom water salinity is assumed ($T = 0$ years), $\epsilon = 0.28$. (b) Case with a covariance time scale $T = 4000$ years, $\epsilon = 0.13$.

pore fluid data still only constrain salinity a few thousand years before present day.

Even when the prior distribution is consistent with the parent (source) distribution of the synthetic $S_{BW}(t)$, larger values of T and smaller values of σ_S^2 lead to more accurate posterior estimates (Fig. 10). When $T = 0$ years and $\sigma_S^2 = 0.05\,\text{g}^2\,\text{kg}^{-2}$, at best the posterior mean estimate resembles the synthetic salinity history in the most recent 8 or 6 ka BP (Fig. 10b). Further back in time, the posterior mean estimate decreasingly resembles the synthetic salinity history, more so the more the synthetic $S_{BW}(t)$ deviates from the prior mean. In the recent past, if the true synthetic $S_{BW}(t)$ is very different from the prior mean, it is easier to recover through the inversion. In the past, if the true synthetic $S_{BW}(t)$ is very different from the prior mean, it is harder to recover through inversion of the measured pore fluid profile data.

The difference between the posterior estimate and an individual random synthetic $S_{BW}(t)$ varies. However, the ensemble difference between the posterior mean and the synthetic time series is reduced relative to the ensemble difference between the prior mean and the synthetic time series, and the degree of reduction is a strong function of T (Fig. 11). With prior assumption $T = 0$ years, the

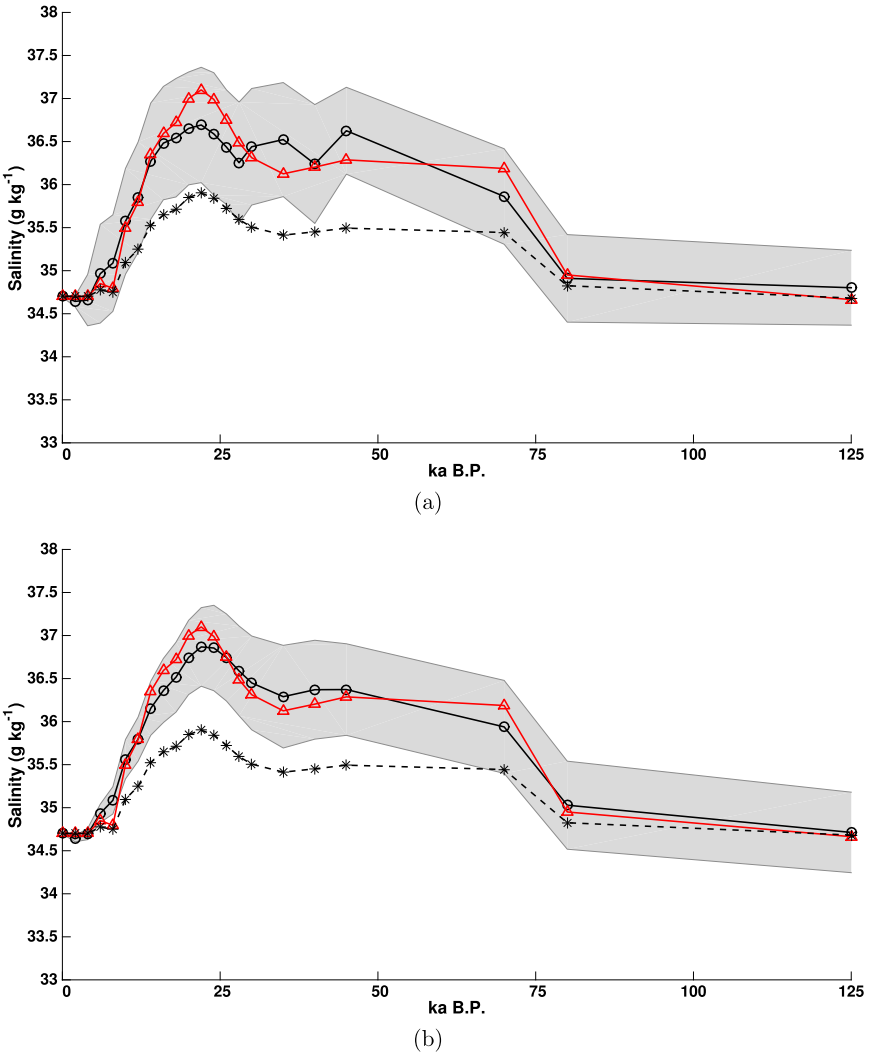

FIG. 9. As in Fig. 8, but with intermediate prior variance. (a) Case where no temporal covariance in bottom water salinity is assumed ($T = 0$ years), $\epsilon = 0.23$. (b) Case with a covariance time scale $T = 4000$ years, $\epsilon = 0.16$.

posterior mean estimate for $S_{\mathrm{BW}}(t)$ is more accurate than the prior estimate between 10 ka BP and the present. With $T = 4000$ years, the posterior mean estimate is more accurate than the prior mean estimate between 20 ka BP and present.

6. Nonlinear problem: Simultaneous inversion of bottom water salinity and diffusivity

The diffusivity in ocean sediment pore waters D_0' is difficult to measure in situ or to estimate from ocean sediment cores. The D_0' values for $[\mathrm{Cl}^-]$ can vary up to an order of magnitude from site to site on the ocean floor. Because the value of D_0' is uncertain, we examine our ability to invert modern measured pore fluid profile data for the value of D_0' simultaneous to $S_{\mathrm{BW}}(t)$. We repeat all of the synthetic examples from section 5 in which D_0' is known, now inverting for D_0' as an unknown parameter with a lognormal prior assumption. The synthetic data are identical to the data inverted for the linear synthetic examples, such that the true value of D_0' is $2.5 \times 10^{-5}\,\mathrm{cm^2\,s^{-1}}$.

a. *Nonlinear inversion of synthetic stretched sea level example with varying prior assumptions*

A larger range of D_0' (here larger than a single, fixed value) in the prior allows for a wider possible range of bottom water histories. With the uninformative prior $\sigma_S^2 = 100\,\mathrm{g^2\,kg^{-2}}$ and T ranging from 0 to 6000 years, the posterior distributions of $S_{\mathrm{BW}}(t)$ are wider than those of the corresponding linear examples. The true value of D_0' is at the low end of the posterior estimate

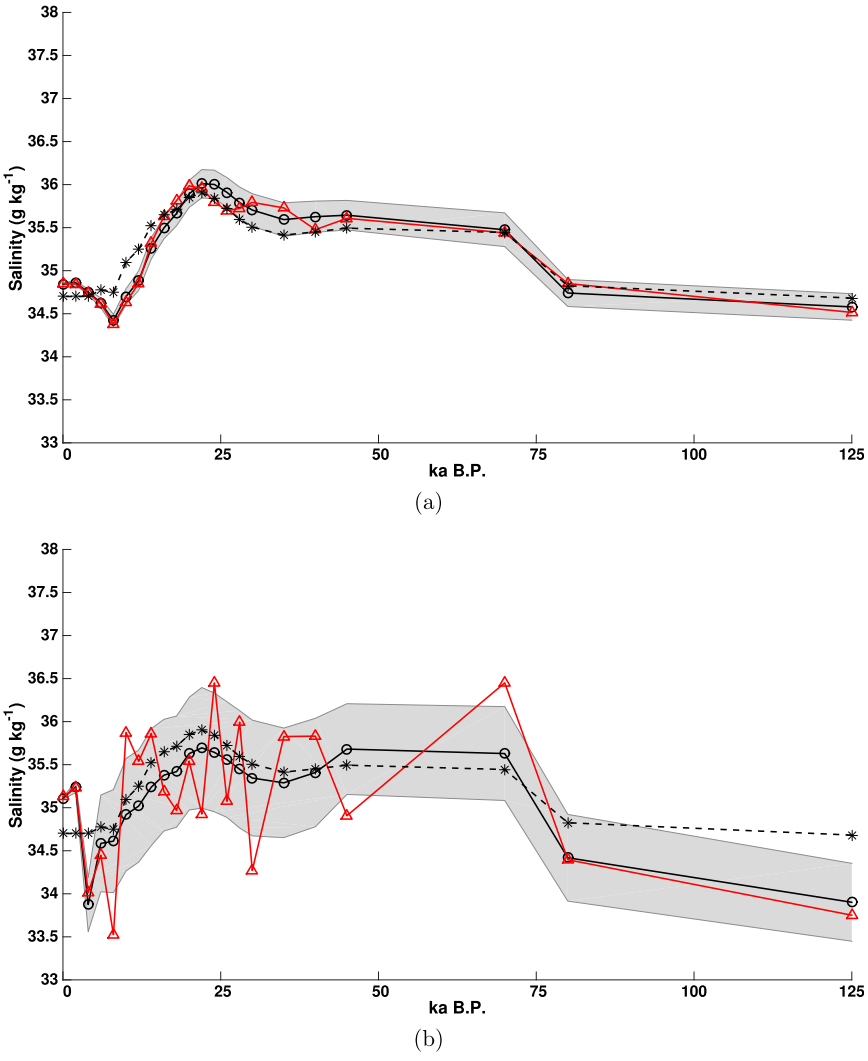

FIG. 10. Synthetic, prior mean, and posterior mean bottom water salinity from representative linear synthetic random ensembles. (a) Variance 0.05 g^2 kg^{-2} and covariance $T = 4000$ years, $\epsilon = 0.10$. (b) Variance 0.5 g^2 kg^{-2} and covariance $T = 0$ years, $\epsilon = 0.60$. Red is the target or true model from which the data were generated. Black circles are the mean of the posterior distribution. Black stars and dashed lines show the mean of the prior distribution.

and does not coincide with the posterior mean (Fig. 12). The posterior mean is also not a good descriptor of the posterior distribution, as the posterior distribution is skewed.

The posterior estimate of D_0' and the posterior estimates of salinities at individual times are correlated (Fig. 13). Near the present, higher-than-modern salinities coincide generally with high D_0', while high salinities further in the past co-occur generally with low D_0'. The pore fluid profile data contain the information that salinity was higher-than-modern at some time in the past. The higher it was recently, the higher D_0' must have been to diffuse away the signal in the sediment (the peak at some depth) to what we measure today. Conversely, if $S_{\mathrm{BW}}(t)$ was higher only in the distant past, D_0' must have been smaller to retain the observed peak in the sediments. However, without independent knowledge of the value of D_0', the data tell us only that salinity was either high recently or high very far in the past. The data cannot distinguish between these two cases. Higher assumed T increases the correlation between D_0' and $S_{\mathrm{BW}}(t)$.

When we solve for D_0' as a parameter in addition to the values of $S_{\mathrm{BW}}(t)$, the frequency content of the posterior mean estimate differs from that of the prior mean and true synthetic $S_{\mathrm{BW}}(t)$. Different values of D_0' enable significantly different $S_{\mathrm{BW}}(t)$ (as judged by their frequency content) to create similar pore fluid profile data.

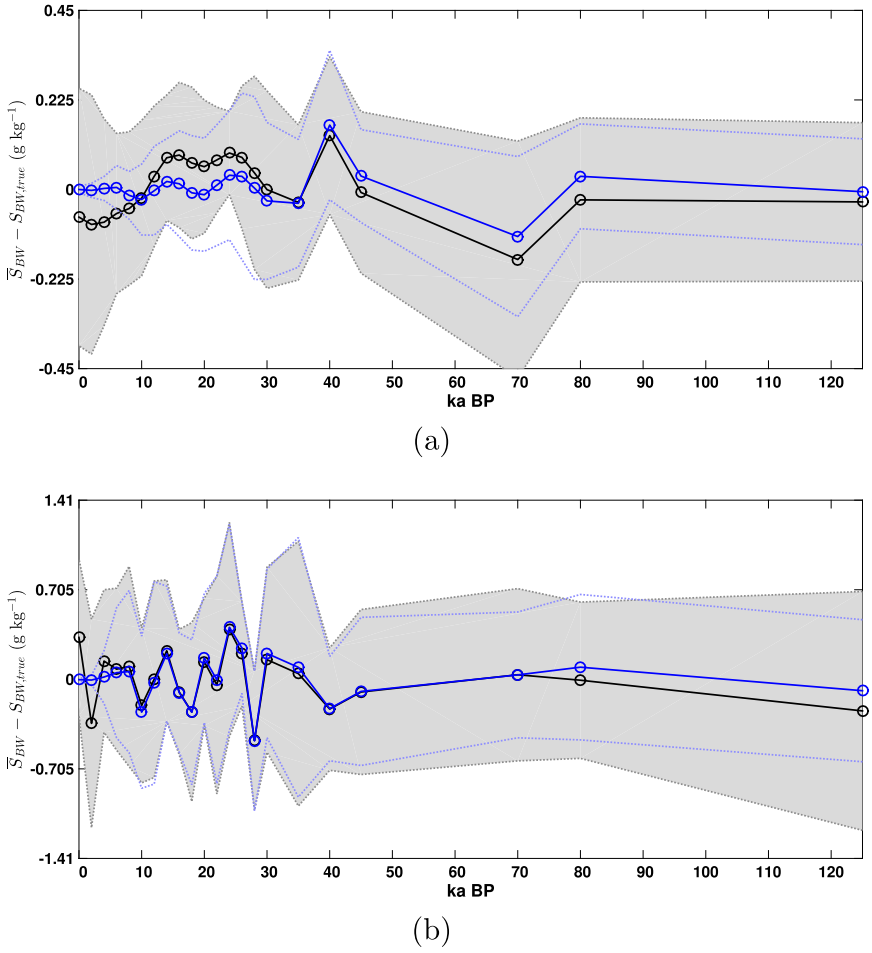

FIG. 11. Difference between the ensemble of random synthetic examples and the prior (black) compared to the difference between the ensemble of random synthetic examples and posterior (blue) distribution means. Values closer to zero indicate better estimates. Shading and dotted lines represent one standard deviation of the ensemble difference: (a) $\sigma_S^2 = 0.05\,\mathrm{g}^2\,\mathrm{kg}^{-2}$, $T = 4000$ years, $\overline{\epsilon} = 0.13$ and (b) $\sigma_S^2 = 0.5\,\mathrm{g}^2\,\mathrm{kg}^{-2}$, $T = 0$ years, $\overline{\epsilon} = 0.58$.

Though the minimum and maximum posterior estimates of D_0' span less than half an order of magnitude, the frequency content of their associated time series are distinct (Fig. 14). That is, the estimated time series of bottom water salinity compensates for the inaccurate estimate of D_0'. With the modern prior assumption ($\sigma_S^2 = 0.05\,\mathrm{g}^2\,\mathrm{kg}^{-2}$) and $T = 0$ or 4000 years, $S_{\mathrm{BW}}(t)$ associated with the minimum D_0' posterior estimate has less power at high frequencies than the mean posterior estimate of $S_{\mathrm{BW}}(t)$, and $S_{\mathrm{BW}}(t)$ associated with the maximum D_0' posterior estimate has more power at high frequencies than the mean posterior estimate of $S_{\mathrm{BW}}(t)$. With the intermediate prior variance assumption ($\sigma_S^2 = 0.05\,\mathrm{g}^2\,\mathrm{kg}^{-2}$), the most significant frequencies in the posterior distribution of $S_{\mathrm{BW}}(t)$ break into different harmonic groups at the extreme values of D_0' (Figs. 14b,d).

b. *Nonlinear inversion for random time series consistent with the Gaussian prior assumption*

We use the identical ensembles of synthetic $S_{\mathrm{BW}}(t)$ and corresponding synthetic data described in section 5b, but now we solve simultaneously for D_0' as an unknown, with the lognormal prior assumption described in sections 3e and 6a.

In these nonlinear inversions, the posterior mean frequency content is a worse estimate of the true frequency content of the synthetic $S_{\mathrm{BW}}(t)$ than in the linear inversions (Fig. 15). The inverse problem is significantly nonlinear in D_0', which means that it is essential to simultaneously solve for D_0' when inverting for $S_{\mathrm{BW}}(t)$. In all of these cases the (peak) power in the inverse solution is more broadly distributed at the maximum D_0' and for least restrictive prior σ_S^2 distributions.

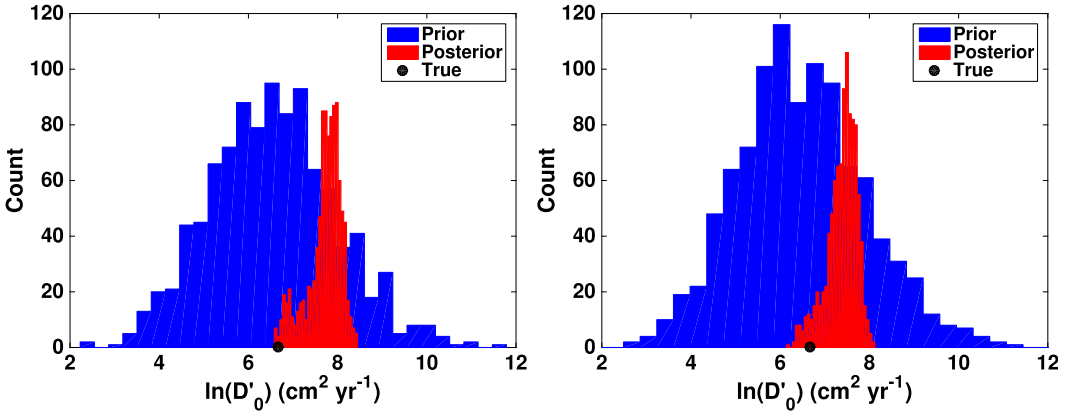

FIG. 12. Prior and posterior distributions of $\ln(D_0')$ for the nonlinear stretched sea level inverse problem with uninformative prior variance ($\sigma_S^2 = 100\,\mathrm{g}^2\,\mathrm{kg}^{-2}$). Gaussian noise of 0.05% is added to the synthetic salinity data before inversion. The black dot in each panel shows the true (target) value of D_0' that is used to generate the data. (a) Case where no temporal covariance in bottom water salinity is assumed ($T = 0$ years), $\epsilon = 1.3$. (b) Case with $T =$ 6000 years, $\epsilon = 0.90$.

As in the stretched sea level examples, the posterior distributions of the estimates of D_0' are wider in the cases when the prior assumed distributions are less informative (Fig. 16). Just as increasing the prior range of D_0' increases the variance of the posterior distribution of $S_{\mathrm{BW}}(t)$, increased prior variance of $S_{\mathrm{BW}}(t)$ leads to increased variance in the posterior estimate of D_0'. However, the posterior distribution of D_0' is better resolved by addition of information in the data than the imposed input prior. The posterior variance of D_0' is smaller by one order of magnitude than its prior variance in all of the cases we considered (Fig. 16). However, the mean posterior estimate of D_0' is not equal to the true value of D_0' used to generate the synthetic data. A greater spread in allowed salinities as imposed through the prior ($\sigma_S^2 = 0.5\,\mathrm{g}^2\,\mathrm{kg}^{-2}$ rather than $0.05\,\mathrm{g}^2\,\mathrm{kg}^{-2}$) allows a greater spread in possible D_0' in the posterior (or vice versa), demonstrating the fundamental covariance between D_0' and the time series of salinities that produce the same data.

7. Discussion and summary

Synthetic examples allow us to determine the maximum information about the past ocean that can be extracted from pore fluid profiles of $\delta^{18}\mathrm{O}$ and $[\mathrm{Cl}^-]$. Without assuming a prior covariance time scale or a narrow range of salinity, the measured pore fluid data constrain the bottom water history between 6 ka BP and present. When the assumed range of possible salinity is narrower ($\sigma_S^2 = 0.05$ or $0.5\,\mathrm{g}^2\,\mathrm{kg}^{-2}$) the measured pore fluid data constrain the bottom water history between 10 ka BP and present. The difference between the distribution of possible inverse solutions and the true bottom water salinity history is a strong function of the assumed time scale of covariance T. Our results demonstrate that modern profiles of pore fluid $\delta^{18}\mathrm{O}$ and $[\mathrm{Cl}^-]$ can constrain the range of salinity and $\delta^{18}\mathrm{O}$ at the LGM only if T is known. When there is no prior assumption of T, the spread of possible salinities at the

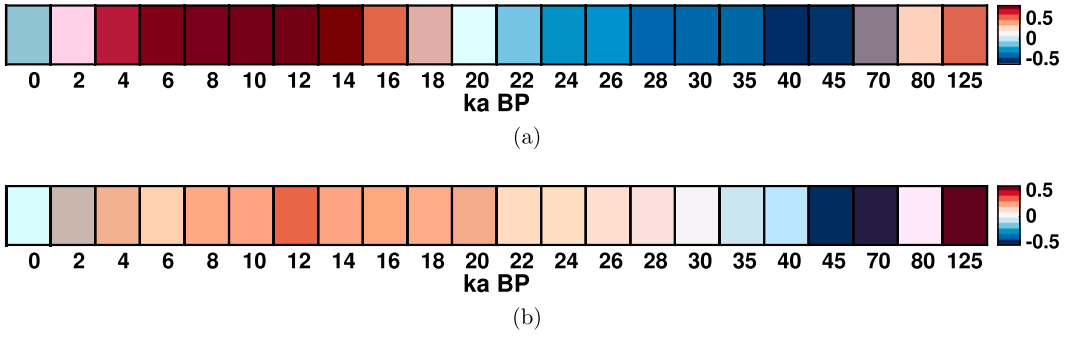

FIG. 13. Correlation coefficients of D_0' vs salinity time series for the nonlinear stretched sea level synthetic example with different assumptions in the prior distribution: (a) $\sigma_S^2 = 0.05\,\mathrm{g}^2\,\mathrm{kg}^{-2}$ and $T = 4000$ years covariance time scale, $\epsilon = 0.23$ and (b) $\sigma_S^2 = 0.5\,\mathrm{g}^2\,\mathrm{kg}^{-2}$ and $T = 0$ years, $\epsilon = 0.28$.

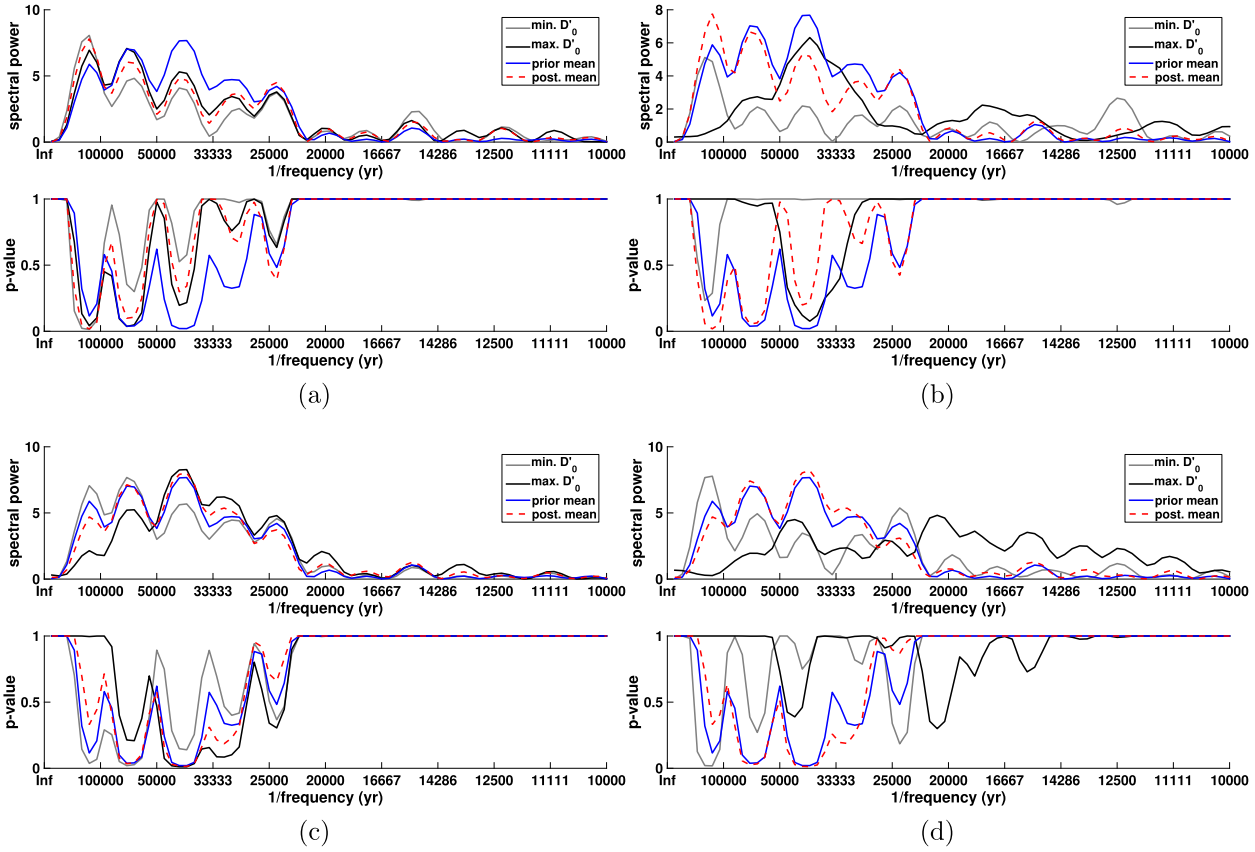

FIG. 14. Lomb–Scargle periodograms for the nonlinear stretched sea level synthetic example of bottom water salinity estimated by inversion (nonlinear problem) for different assumptions about the prior distribution. (a) Salinity variance $\sigma_S^2 = 0.05\,\mathrm{g}^2\,\mathrm{kg}^{-2}$ and covariance time scale $T = 0$ years, $\epsilon = 0.34$; (b) $\sigma_S^2 = 0.5\,\mathrm{g}^2\,\mathrm{kg}^{-2}$ and $T = 0$ years, $\epsilon = 0.28$; (c) $\sigma_S^2 = 0.05\,\mathrm{g}^2\,\mathrm{kg}^{-2}$ and $T = 4000$ years, $\epsilon = 0.23$; and (d) $\sigma_S^2 = 0.5\,\mathrm{g}^2\,\mathrm{kg}^{-2}$ and $T = 4000$ years, $\epsilon = 0.26$.

LGM is equivalent to the initial guess or the variance of the prior distribution. While the absolute values of salinities prior to 10 ka BP are unconstrained by the pore fluid data, the data do constrain the correlation between the salinities at different times in the past. This information about correlation is useful because, combined with other independent data, it could narrow the range of past salinity.

Previous work suggested that the diffusivity coefficient D_0' could be determined from a scaling argument separately from the bottom water salinity history. Here we show that the inverse estimate of D_0' strongly covaries with the inverse estimate of bottom water salinity. Over a narrow, physically realistic range of D_0', the correlation between salinities at different times in the inverse estimate changes dramatically. For this reason, when we estimate bottom water salinity histories from measured pore fluid profiles, D_0' must be included as an unknown parameter.

In all the synthetic cases described here, the bottom boundary condition (vertical gradient of S at $z = 350$ m) and the initial condition (vertical profile of S from the sediment–water interface at $z = 0$ m to $z = 350$ m at 125 000 years ago) are fixed and assumed to be known. We assumed that the cyclical nature of glaciations and deglaciations caused the data profile at 125 ka BP (our initial condition) to be equivalent to the modern measurement profile. We also assumed that the gradient boundary condition at the bottom of the sediment column is constant over the time period of integration and that it can be estimated from the slope of the measured pore fluid data over the final (bottom) tens of meters in the sediment column.

Our inverse framework allows us to relax these assumptions and instead solve for the initial condition and bottom boundary condition as additional unknown parameters. Our preliminary work in this area (see, e.g., Miller 2014) confirms our intuition that, in general, an increased number of free parameters in an ill-posed problem such as this one always increases the uncertainty of the posterior parameter distributions. We make many other assumptions in our advection–diffusion model [Eq. (4)], such as the assumption of steady-state compaction and the

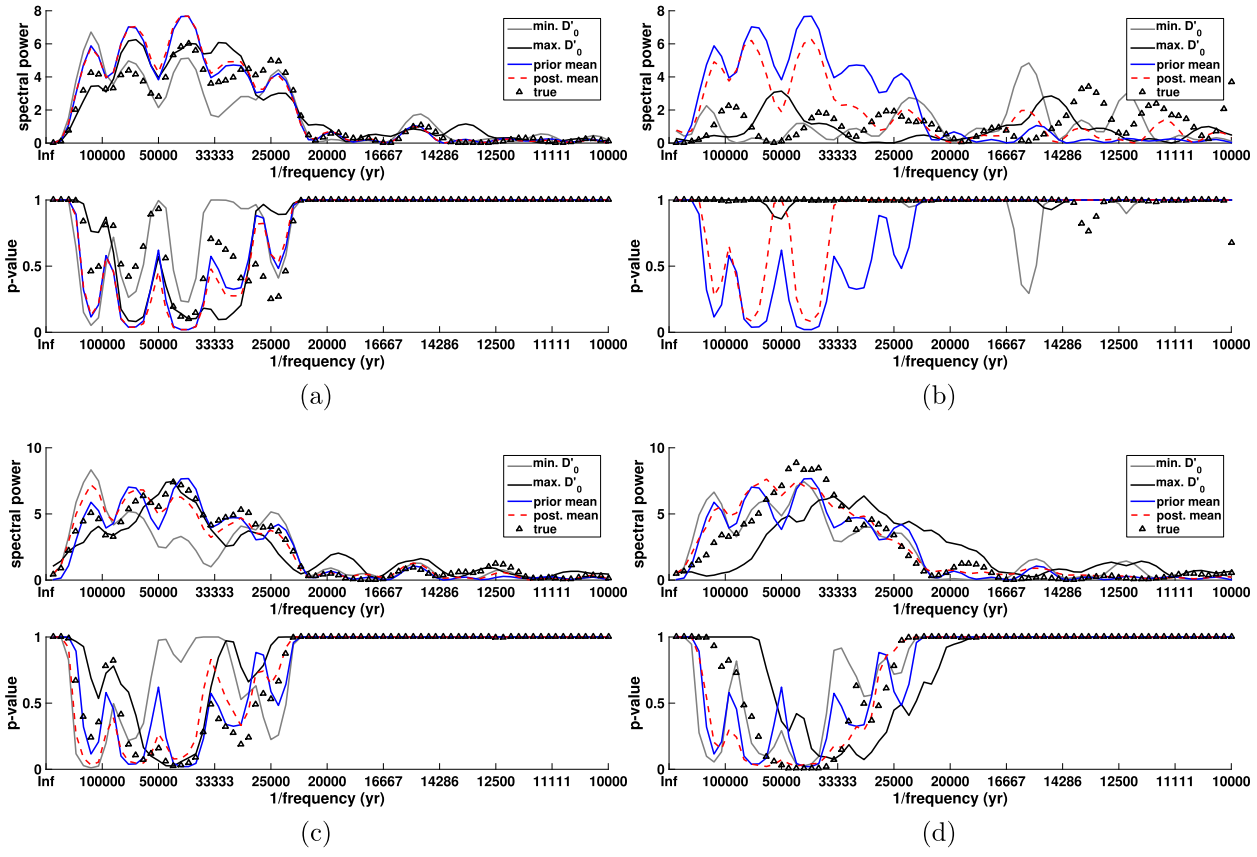

FIG. 15. Lomb–Scargle periodograms for representative examples from the nonlinear random ensemble synthetic examples of bottom water salinity estimated by inversion (nonlinear problem) for different assumptions about the prior distribution. (a) Salinity variance $\sigma_S^2 = 0.05\,\mathrm{g}^2\,\mathrm{kg}^{-2}$ and covariance time scale $T = 0$ years, $\epsilon = 0.23$; (b) $\sigma_S^2 = 0.5\,\mathrm{g}^2\,\mathrm{kg}^{-2}$ and $T = 0$ years, $\epsilon = 0.68$; (c) $\sigma_S^2 = 0.05\,\mathrm{g}^2\,\mathrm{kg}^{-2}$ and $T = 4000$ years, $\epsilon = 0.13$; and (d) $\sigma_S^2 = 0.5\,\mathrm{g}^2\,\mathrm{kg}^{-2}$ and $T = 4000$ years, $\epsilon = 0.47$.

assumed relationship between sediment tortuosity and porosity. If these assumptions were relaxed, it is likely that the uncertainty in bottom water salinity and $\delta^{18}O$ deduced from pore water profiles would further inflate.

Adkins et al. (2002) relied on stretching and shrinking the salinity history scaled to a composite benthic $\delta^{18}O_c$ and mean sea level history, rather than allowing the salinities at each time to vary independently, and this is

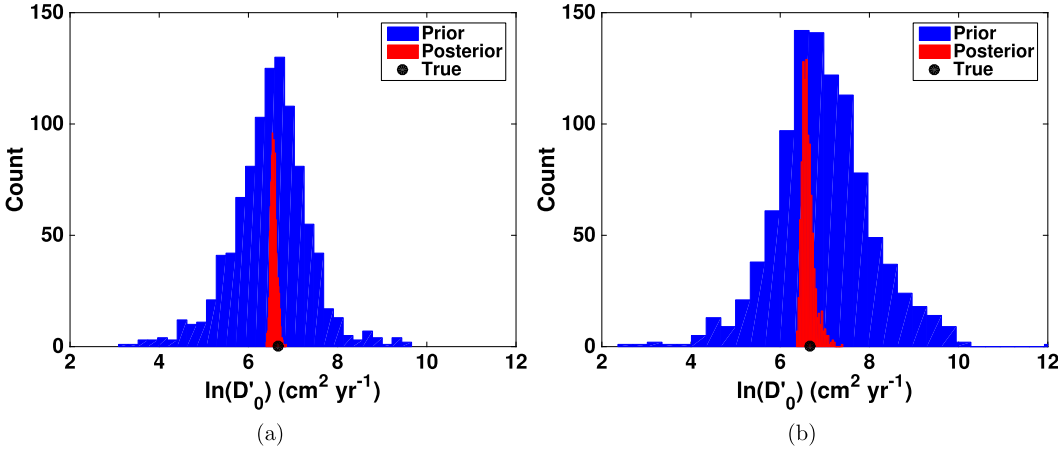

FIG. 16. Prior and posterior distributions of $\ln(D_0')$ from representative examples from the nonlinear synthetic random ensembles. (a) Salinity variance $\sigma_S^2 = 0.05\,\mathrm{g}^2\,\mathrm{kg}^{-2}$ and covariance time scale $T = 4000$ years, $\epsilon = 0.13$; (b) $\sigma_S^2 = 0.5\,\mathrm{g}^2\,\mathrm{kg}^{-2}$ and $T = 0$ years, $\epsilon = 0.68$.

equivalent to assuming that the salinity covariance time scale T is 4000 years or longer. We have shown here that the variance of the inverse estimate of salinity at the LGM (assuming the LGM occurred around 20 ka BP) is entirely determined by the prior assumption of σ_S^2 and T. Therefore, the error reported in Schrag and DePaolo (1993), Schrag et al. (1996), Adkins and Schrag (2001), Paul et al. (2001), Adkins et al. (2002), Schrag et al. (2002), Malone et al. (2004), and Lado Insua et al. (2014) may underestimate the true uncertainty of estimated LGM deep ocean salinity and $\delta^{18}O$.

Adkins and Schrag (2003) investigated the sensitivity of estimating LGM salinity to various assumptions about the bottom water salinity history, the diffusivity of $[Cl^-]$, the effective advective velocity of $[Cl^-]$, and the initial condition pore fluid profile. They concluded that the overall uncertainty in the relative difference between LGM and present salinity was 0.1%–0.5% (out of 3.5%). Their approach involved small perturbations around a fixed value, varying only one parameter at a time. Our approach allows us to vary the parameters simultaneously and therefore explore the inverse solution space more completely. We find that salinities, diffusivity, and initial conditions can compensate for each other. This ability to compensate increases the uncertainty on any one parameter.

Previous authors (Lado Insua et al. 2014; Malone et al. 2004; Adkins et al. 2002; Schrag et al. 2002; Adkins and Schrag 2001; Paul et al. 2001; Schrag et al. 1996; Schrag and DePaolo 1993; McDuff 1985) who have reconstructed LGM salinity and $\delta^{18}O$ from pore fluid profiles have all assumed that the bottom water salinity history was a scaled version of the benthic $\delta^{18}O_c$ history or the sea level curve. Such a scaling imposes a specific set of temporal correlations on the bottom water history. It is difficult to justify assuming that the temporal correlation of salinity at a deep ocean site exactly matches that of the changing sea level or of $\delta^{18}O_c$. The temporal correlation in $\delta^{18}O$ is only equivalent to that in a benthic $\delta^{18}O_c$ record if the proportion of changes in $\delta^{18}O$ to temperature remains constant over time. Without this assumed temporal correlation, the uncertainty of the LGM salinity and $\delta^{18}O$ inferred from pore fluids is greater. If we can narrow the likely range of temporal correlation further, as is done through assumption in previous work, we can use the pore fluid profiles to help constrain the bottom water salinity and $\delta^{18}O$ histories from the LGM through the deglaciation to the present. Increased prior information on T could be gained from analyzing temporal correlations in benthic foraminiferal records of bottom water properties in the same cores.

Acknowledgments. M.D.M. thanks William Jenkins for introduction to the Lomb–Scargle periodogram and Eli Tziperman for many helpful discussions and constructive reviews of drafts of this manuscript.

REFERENCES

Adkins, J. F., and D. P. Schrag, 2001: Pore fluid constraints on deep ocean temperature and salinity during the last glacial maximum. *Geophys. Res. Lett.,* **28,** 771–774, doi:10.1029/2000GL011597.

——, and ——, 2003: Reconstructing Last Glacial Maximum bottom water salinities from deep-sea sediment pore fluid profiles. *Earth Planet. Sci. Lett.,* **216,** 109–123, doi:10.1016/S0012-821X(03)00502-8.

——, K. McIntyre, and D. P. Schrag, 2002: The salinity, temperature and $\delta^{18}O$ of the glacial deep ocean. *Science,* **298,** 1769–1773, doi:10.1126/science.1076252.

Ascher, U. M., S. J. Ruuth, and B. T. R. Wetton, 1995: Implicit-explicit methods for time-dependent partial differential equations. *SIAM J. Numer. Anal.,* **32,** 797–823, doi:10.1137/0732037.

Bard, E., B. Hamelin, and R. G. Fairbanks, 1990a: U-Th ages obtained by mass spectrometry in corals from Barbados: Sea level during the past 130,000 years. *Nature,* **346,** 456–458, doi:10.1038/346456a0.

——, ——, ——, and A. Zindler, 1990b: Calibration of the ^{14}C timescale over the past 30,000 years using mass spectrometric U-Th ages from Barbados corals. *Nature,* **345,** 405–410, doi:10.1038/345405a0.

——, ——, M. Arnold, L. Montaggioni, G. Cabioch, G. Faure, and F. Rougerie, 1996: Deglacial sea-level record from Tahiti corals and the timing of global meltwater discharge. *Nature,* **382,** 241–244, doi:10.1038/382241a0.

Bellman, R. E., 1957: *Dynamic Programming.* Princeton University Press, 384 pp.

Berner, R. A., 1980: *Early Diagenesis: A Theoretical Approach.* Princeton University Press, 241 pp.

Boudreau, B. P., 1997: *Diagenetic Models and Their Implementation: Modelling Transport and Reaction in Aquatic Sediments.* Springer-Verlag, 414 pp.

Broecker, W., and S. Barker, 2007: A 190‰ drop in atmosphere's $\Delta^{14}C$ during the "Mystery Interval" (17.5 to 14.5 kyr). *Earth Planet. Sci. Lett.,* **256,** 90–99, doi:10.1016/j.epsl.2007.01.015.

Chappell, J., and N. J. Shackleton, 1986: Oxygen isotopes and sea level. *Nature,* **324,** 137–140, doi:10.1038/324137a0.

——, A. Omura, T. Esat, M. McCulloch, J. Pandolfi, Y. Ota, and B. Pillans, 1996: Reconciliation of late Quaternary sea levels derived from coral terraces at Huon Peninsula with deep sea oxygen isotope records. *Earth Planet. Sci. Lett.,* **141,** 227–236, doi:10.1016/0012-821X(96)00062-3.

Charles, C. D., J. Lynch-Stieglitz, U. S. Ninnemann, and R. G. Fairbanks, 1996: Climate connections between the hemisphere revealed by deep sea sediment core/ice core correlations. *Earth Planet. Sci. Lett.,* **142,** 19–27, doi:10.1016/0012-821X(96)00083-0.

Chen, J. H., H. A. Curran, B. White, and G. J. Wasserburg, 1991: Precise chronology of the last interglacial period: ^{234}U-^{230}Th data from fossil coral reefs in the Bahamas. *Geol. Soc. Amer. Bull.,* **103,** 82–97, doi:10.1130/0016-7606(1991)103<0082:PCOTLI>2.3.CO;2.

Clark, P. U., and Coauthors, 2009: The Last Glacial Maximum. *Science,* **325,** 710–714, doi:10.1126/science.1172873.

Collins, L. B., Z. R. Zhu, K.-H. Wyrwoll, B. G. Hatcher, P. E. Playford, J. H. Chen, A. Eisenhauer, and G. J. Wasserburg, 1993a: Late Quaternary evolution of coral reefs on a cool-water carbonate margin: The Abrolhos Carbonate Platforms, southwest Australia. *Mar. Geol.,* **110,** 203–212, doi:10.1016/0025-3227(93)90085-A.

——, and Coauthors, 1993b: Holocene growth history of a reef complex on a cool-water carbonate margin: Easter Group of the Houtman Abrolhos, Eastern Indian Ocean. *Mar. Geol.,* **115,** 29–46, doi:10.1016/0025-3227(93)90073-5.

Dansgaard, W., and H. Tauber, 1969: Glacier oxygen-18 content and Pleistocene ocean temperatures. *Science,* **166,** 499–502, doi:10.1126/science.166.3904.499.

Duplessy, J.-C., E. Bard, M. Arnold, N. J. Shackleton, J. Duprat, and L. Labeyrie, 1991: How fast did the ocean-atmosphere system run during the last deglaciation? *Earth Planet. Sci. Lett.,* **103,** 27–40, doi:10.1016/0012-821X(91)90147-A.

——, L. Labeyrie, and C. Waelbroeck, 2002: Constraints on the ocean oxygen isotopic enrichment between the Last Glacial Maximum and the Holocene: Paleoceanographic implications. *Quat. Sci. Rev.,* **21,** 315–330, doi:10.1016/S0277-3791(01)00107-X.

Edwards, R. L., F. W. Taylor, and G. J. Wasserburg, 1988: Dating earthquakes with high-precision Thorium-230 ages of very young corals. *Earth Planet. Sci. Lett.,* **90,** 371–381, doi:10.1016/0012-821X(88)90136-7.

——, J. W. Beck, G. S. Burr, D. J. Donahue, J. M. A. Chappell, A. L. Bloom, E. R. M. Druffel, and F. W. Taylor, 1993: A large drop in atmospheric $^{14}C/^{12}C$ and reduced melting in the Younger Dryas, documented with ^{230}Th ages of corals. *Science,* **260,** 962–968, doi:10.1126/science.260.5110.962.

Emiliani, C., 1966: Paleotemperature analysis of Caribbean cores P6304-8 and P6304-9 and a generalized temperature curve for the past 425,000 years. *J. Geol.,* **74,** 109–126, doi:10.1086/627150.

Esat, T. M., M. T. McCulloch, J. Chappell, B. Pillans, and A. Omura, 1999: Rapid fluctuations in sea level recorded at Huon Peninsula during the penultimate deglaciation. *Science,* **283,** 197–201, doi:10.1126/science.283.5399.197.

Fairbanks, R. G., 1989: A 17,000-year glacio-eustatic sea level record: Influence of glacial melting rates on the Younger Dryas event and deep-ocean circulation. *Nature,* **342,** 637–642, doi:10.1038/342637a0.

Ferrari, R., and C. Wunsch, 2009: Ocean circulation kinetic energy: Reservoirs, sources, and sinks. *Annu. Rev. Fluid Mech.,* **41,** 253–282, doi:10.1146/annurev.fluid.40.111406.102139.

Gallup, C. D., R. L. Edwards, and R. G. Johnson, 1994: The timing of high sea levels over the past 200,000 years. *Science,* **263,** 796–800, doi:10.1126/science.263.5148.796.

Gebbie, G., 2012: Tracer transport timescales and the observed Atlantic-Pacific lag in the timing of the Last Termination. *Paleoceanography,* **27,** PA3225, doi:10.1029/2011PA002273.

——, and P. Huybers, 2006: Meridional circulation during the Last Glacial Maximum explored through a combination of South Atlantic $\delta^{18}O$ observations and a geostrophic inverse model. *Geochem. Geophys. Geosyst.,* **7,** Q11N07, doi:10.1029/2006GC001383.

Gersonde, R., and Coauthors, 1999: Southern Ocean paleoceanography. *Proc. Ocean Drill. Program: Initial Rep.,* **177,** doi:10.2973/odp.proc.ir.177.1999.

Hansen, P. C., 1998: *Rank-Deficient and Discrete Ill-Posed Problems.* Society for Industrial and Applied Mathematics, 243 pp.

Hodell, D. A., K. A. Venz, C. D. Charles, and U. S. Ninnemann, 2003: Pleistocene vertical carbon isotope and carbonate gradients in the South Atlantic sector of the Southern Ocean. *Geochem. Geophys. Geosyst.,* **4,** 1004, doi:10.1029/2002GC000367.

Huettel, M., and I. T. Webster, 2001: Porewater flow in permeable sediments. *The Benthic Boundary Layer: Transport Processes and Biogeochemistry,* B. P. Boudreau and B. B. Jørgensen, Eds., Oxford University Press, 144–179.

Judd, A., and M. Hovland, 2007: *Seabed Fluid Flow.* Cambridge University Press, 492 pp.

Lado Insua, T., A. J. Spivack, D. Graham, S. D'Hondt, and K. Moran, 2014: Reconstruction of Pacific Ocean bottom water salinity during the Last Glacial Maximum. *Geophys. Res. Lett.,* **41,** 2914–2920, doi:10.1002/2014GL059575.

Lamy, F., J. Kaiser, U. Ninnemann, D. Hebbeln, H. W. Arz, and J. Stoner, 2004: Antarctic timing of surface water changes off Chile and Patagonian Ice Sheet response. *Science,* **304,** 1959–1962, doi:10.1126/science.1097863.

LeGrand, P., and C. Wunsch, 1995: Constraints from paleotracer data on the North Atlantic circulation during the Last Glacial Maximum. *Paleoceanography,* **10,** 1011–1045, doi:10.1029/95PA01455.

LeGrande, A. N., and G. A. Schmidt, 2006: Global gridded data set of the oxygen isotopic composition in seawater. *Geophys. Res. Lett.,* **33,** L12604, doi:10.1029/2006GL026011.

Li, Y.-H., and S. Gregory, 1974: Diffusion of ions in sea water and in deep-sea sediments. *Geochim. Cosmochim. Acta,* **38,** 703–714, doi:10.1016/0016-7037(74)90145-8.

Ludwig, K. R., D. R. Muhs, K. R. Simmons, R. B. Halley, and E. A. Shinn, 1996: Sea-level records at ~80 ka from tectonically stable platforms: Florida and Bermuda. *Geology,* **24,** 211–214, doi:10.1130/0091-7613(1996)024<0211:SLRAKF>2.3.CO;2.

Lund, D. C., J. F. Adkins, and R. Ferrari, 2011: Abyssal Atlantic circulation during the Last Glacial Maximum: Constraining the ratio between transport and vertical mixing. *Paleoceanography,* **26,** PA1213, doi:10.1029/2010PA001938.

Lynch-Stieglitz, J., 2004: Hemispheric asynchrony of abrupt climate change. *Science,* **304,** 1919–1920, doi:10.1126/science.1100374.

Malone, M. J., J. B. Martin, J. Schonfeld, U. S. Ninnemann, D. Nurnberg, and T. S. White, 2004: The oxygen isotopic composition and temperature of Southern Ocean bottom waters during the Last Glacial Maximum. *Earth Planet. Sci. Lett.,* **222,** 275–283, doi:10.1016/j.epsl.2004.02.027.

Marchal, O., and W. B. Curry, 2008: On the abyssal circulation in the glacial Atlantic. *J. Phys. Oceanogr.,* **38,** 2014–2037, doi:10.1175/2008JPO3895.1.

MARGO Project Members, 2009: Constraints on the magnitude and patterns of cooling at the Last Glacial Maximum. *Nat. Geosci.,* **2,** 127–132, doi:10.1038/ngeo411.

McDuff, R. E., 1985: The chemistry of interstitial waters, Deep Sea Drilling Project Leg 86. *Initial Reports of the Deep Sea Drilling Project,* Vol. 86, G. R. Heath et al., Eds., U.S. Government Printing Office, 675–687, doi:10.2973/dsdp.proc.86.131.1985.

Miller, M. D., 2014: The deep ocean density structure at the Last Glacial Maximum: What was it and why? Ph.D. dissertation, California Institute of Technology, 230 pp.

——, J. F. Adkins, D. Menemenlis, and M. P. Schodlok, 2012: The role of ocean cooling in setting glacial southern source bottom water salinity. *Paleoceanography,* **27,** PA3207, doi:10.1029/2012PA002297.

Minson, S. E., M. Simons, and J. L. Beck, 2013: Bayesian inversion for finite fault earthquake source models I—Theory and algorithm. *Geophys. J. Int.,* **194,** 1701–1726, doi:10.1093/gji/ggt180.

Mix, A. C., 1987: The oxygen-isotope record of glaciation. *North America and Adjacent Oceans during the Last Deglaciation,* W. F. Ruddiman and H. E. Wright Jr., Eds., Geological Society of America, 111–135.

Pahnke, K., and R. Zahn, 2005: Southern Hemisphere water mass conversion linked with North Atlantic climate variability. *Science,* **307,** 1741–1746, doi:10.1126/science.1102163.

Paul, H. A., S. M. Bernasconi, D. W. Schmid, and J. A. Mckenzie, 2001: Oxygen isotopic composition of the Mediterranean Sea since the Last Glacial Maximum: Constraints from pore water analyses. *Earth Planet. Sci. Lett.,* **192,** 1–14, doi:10.1016/S0012-821X(01)00437-X.

Robinson, L. F., J. F. Adkins, L. D. Keigwin, J. Southon, D. P. Fernandez, S.-L. Wang, and D. S. Scheirer, 2005: Radiocarbon variability in the western North Atlantic during the last deglaciation. *Science,* **310,** 1469–1473, doi:10.1126/science.1114832.

Schrag, D. P., and D. J. DePaolo, 1993: Determination of $\delta^{18}O$ of seawater in the deep ocean during the Last Glacial Maximum. *Paleoceanography,* **8,** 1–6, doi:10.1029/92PA02796.

——, G. Hampt, and D. Murray, 1996: Pore fluid constraints on the temperature and oxygen isotopic composition of the glacial ocean. *Science,* **272,** 1930–1932, doi:10.1126/science.272.5270.1930.

——, J. Adkins, K. McIntyre, J. Alexander, D. Hodell, C. Charles, and J. McManus, 2002: The oxygen isotopic composition of seawater during the Last Glacial Maximum. *Quat. Sci. Rev.,* **21,** 331–342, doi:10.1016/S0277-3791(01)00110-X.

Schmidt, G. A., G. R. Bigg, and E. J. Rohling, 1999: Global Seawater Oxygen-18 Database–v1.21. NASA Goddard Institute for Space Studies, accessed 12 September 2012. [Available online at http://data.giss.nasa.gov/o18data/.]

Shackleton, N. J., 1967: Oxygen isotope analyses and Pleistocene temperatures re-assessed. *Nature,* **215,** 15–17, doi:10.1038/215015a0.

Skinner, L., and N. Shackleton, 2005: An Atlantic lead over Pacific deep-water change across Termination I: Implications for the application of the marine isotope stage stratigraphy. *Quat. Sci. Rev.,* **24,** 571–580, doi:10.1016/j.quascirev.2004.11.008.

Spinelli, G. A., E. R. Giambalvo, and A. T. Fisher, 2004: Hydrologic properties and distribution of sediments. *Hydrogeology of the Oceanic Lithosphere,* E. Davis and H. Elderfield, Eds., Cambridge University Press, 151–188.

Stein, M., G. J. Wasserburg, P. Aharon, J. H. Chen, Z. R. Zhu, A. Bloom, and J. Chappell, 1993: TIMS U-series dating and stable isotopes of the last interglacial event in Papua New Guinea. *Geochim. Cosmochim. Acta,* **57,** 2541–2554, doi:10.1016/0016-7037(93)90416-T.

Stirling, C. H., T. M. Esat, M. T. McCulloch, and K. Lambeck, 1995: High-precision U-series dating of corals from Western Australia and implications for the timing and duration of the Last Interglacial. *Earth Planet. Sci. Lett.,* **135,** 115–130, doi:10.1016/0012-821X(95)00152-3.

——, ——, K. Lambeck, and M. T. McCulloch, 1998: Timing and duration of the Last Interglacial: Evidence for a restricted interval of widespread coral reef growth. *Earth Planet. Sci. Lett.,* **160,** 745–762, doi:10.1016/S0012-821X(98)00125-3.

Szabo, B. J., K. R. Ludwig, D. R. Muhs, and K. R. Simmons, 1994: Thorium-230 ages of corals and duration of the Last Interglacial sea-level high stand on Oahu, Hawai'i. *Science,* **266,** 93–96, doi:10.1126/science.266.5182.93.

Tarantola, A., 2005: *Inverse Problem Theory and Methods for Model Parameter Estimation.* Society for Industrial and Applied Mathematics, 352 pp.

Wang, J. H., C. V. Robinson, and I. S. Edelman, 1953: Self-diffusion and structure of liquid water. III. Measurement of the self-diffusion of liquid water with H^2, H^3 and O^{18} as tracers. *J. Amer. Chem. Soc.,* **75,** 466–470, doi:10.1021/ja01098a061.

Wunsch, C., and P. Heimbach, 2008: How long to oceanic tracer and proxy equilibrium? *Quat. Sci. Rev.,* **27,** 637–651, doi:10.1016/j.quascirev.2008.01.006.

Zika, J. D., B. M. Sloyan, and T. J. McDougall, 2009: Diagnosing the Southern Ocean overturning from tracer fields. *J. Phys. Oceanogr.,* **39,** 2926–2940, doi:10.1175/2009JPO4052.1.

——, T. J. McDougall, and B. M. Sloyan, 2010: Weak mixing in the eastern North Atlantic: An application of the tracer-contour inverse method. *J. Phys. Oceanogr.,* **40,** 1881–1893, doi:10.1175/2010JPO4360.1.